NASA Contractor Report 180863

# Stress Rupture Behavior of Silicon Carbide Coated, Low Modulus Carbon/Carbon Composites

Gary A. Rozak and John F. Wallace
*Case Western Reserve University*
*Cleveland, Ohio*

January 1988

Prepared for
Lewis Research Center
Under Grant NAG3-464

National Aeronautics and
Space Administration

TABLE OF CONTENTS

The disadvantages of c/c, in addition to the oxidation problem, are low thermal expansion, expensive fabrication procedures, and poor off axis properties. The strength perpendicular to the fiber directions in the composites are as low as 360 psi (2.5 MPa) [2]. The shear strength of the composite is also as low as 2000 psi (14 MPa) [2]. The fabrication of c/c involves long processing times at high temperatures and consequently is expensive. The thermal expansion of c/c is small and makes it difficult to apply a successful coating because the thermal expansions of most coating materials are greater than that of c/c. The disadvantages of expensive fabrication and low off axis properties will become secondary if a successful coating system is developed.

The following subjects are reviewed: 1) background of c/c, 2) fabrication of c/c, 3) oxidation of carbon, 5) oxidation protection methods for c/c, and 6) mechanical testing of c/c in flexure.

## Background

The first carbon matrix composite was inadvertantly produced in the late 1950's during ablation studies of composites with oxide fibers and a polymeric matrix [1]. The pyrolization of this composite yielded a carbon char as the matrix when a crucible was accidentally covered. Later, the oxide fibers were replaced by a carbon fiber in the composite and the first c/c was the result. The development of c/c in the succeeding years was directed by its usage in aerospace [1].

Aerospace applications of c/c began with single life mission missiles and evolved into multimission components on the space shuttle. A c/c replaced bulk graphite as the material for the nose cone and exhaust nozzle structure on single mission missiles for better performance [1]. A reinforced c/c (RCC), low strength and low modulus c/c, is employed on the space shuttle for such applications as the nose cone and leading edges [3]. These parts experience the greatest heat in re-entry from orbit and require good ablation resistant properties [3].

The reuse of the shuttle requires an oxidation protection system for the c/c to extend its life. The RCC material has a silicon carbide coating for protection [3]. The coating is applied to the parts by a pack cementation conversion of the surface to silicon carbide. The coating is further enhanced by a surface layer of tetra ethyl ortho silicate (TEOS), which is brushed onto the surface and then cured to form a silicon dioxide layer.

The improvement in the mechanical properties of c/c was the next evolutionary step. Low modulus carbon fibers were replaced by higher modulus fibers and resulted in an Advanced c/c (ACC). The strength of ACC is three times greater than RCC and the modulus is six times greater. Applications of ACC are being pursued in the space shuttle and hypersonic aircraft [3]. The application of coated ACC as jet engine exhaust nozzle liners [3] was successful for ground based test in a F100 turbine engine. The success of this program prompted the pursuit of coated ACC materials as liners for the two dimensional (2-D) exhaust nozzle liner program.

Oxidation problems, experienced on the coated ACC materials in the 2-D exhaust nozzle program, resulted in an increase of research in inhibited c/c (ICC). These c/c incorporate chemicals, viz. boron, and silicon, in the matrix that inhibit the oxidation of carbon by blocking oxidation sites.

Usages of c/c are not limited to aerospace applications. Carbon/carbon has been used successfully as biomedical implants because of the biological chemical inertness of carbon. Carbon/carbon is finding use as an asbestos replacement in vehicle brakes because of its friction and wear characteristics. Further applications of c/c are described in a recent review article by Fitzer [4].

## Fabrication of Carbon/Carbon

The fabrication of c/c requires a choice of composite precursor materials for the fibers and matrix. The composite fabrication entails the lay up, impregnation, carbonization, and densification. More details are found in a review by Stoller et al [5].

One method of forming the matrix of c/c is the pyrolization of organic precursors. The available polymeric precursors to the matrix consist of high char forming polymers, e.g. phenolic resins, furfural and pitches [6]. The matrix is amorphous carbon after the carbonization cycle. Further elevated temperature processing above 3600°F (2000°C) will convert the matrix to graphite in the case of the pitch and alcohol precursors, whereas the phenolic resins remain amorphous after this heat treatment [5].

Deposition of pyrolitic graphite by chemical vapor deposition (CVD) methods is the alternative route of matrix formation and

involves a reaction of a hydrocarbon gas that deposits carbon on the matrix. The properties of this graphite is dependent on the deposition temperature and rate. This method can also be employed to densify the matrix of charred matrix composites.

Commercially available carbon fibers are derived from different organic precursors -- rayon, pitch, and polyacrylonitrile (PAN) -- all of which undergo similar processing steps to arrive at the final properties. Other polymers, such as phenolics, phenol formaldehyde, resins, and polyimides can be used as fiber precursors but are not commercially available. The processing of the fibers involves the spinning of the precursor into fibers and yarns, stabilization, and carbonization. The fiber yarns are stabilized with a cure at moderate temperature of 300° to 500° (150° to 260°C). Carbonization is an additional heat treatment in a controlled atmosphere to decompose the precursor and yield carbon fibers. The strength and modulus of elasticity of the fibers can be improved along the axis of the fiber by a stretching procedure during production. This can increase the modulus of a rayon fiber from 4 Msi (28 GPa) to above 50 Msi (345 GPa); strength is increased from 100 ksi (700 MPa) to over 300 ksi (2100 MPa) [5]. Donnett and Bansal [7] give greater details on fiber fabrication.

Carbon/carbon is fabricated in many fiber orientations. Some applications employ chopped fibers in random orientation or carbon felts as the base preforms. Woven fabrics of carbon yarns are common for aerospace application. Cloths are easier to handle and the lay up is faster [8]. The shear strengths in the plane of the ply is better

with a woven fabric than unidirectional plies of yarns which are laid up orthogonally [9]. The carbon fabric consists of yarns running orthogonal to each other. The yarn directions are called the warp and fill and the warp yarns are stitched, i.e. a crossover, by the fill yarns. Consequently, the warp yarns are generally straighter and stronger than those in the fill direction.

Some of the available weave types are the plain, five and eight harness satin, and unbalanced. The plain weave is fabricated such that fill yarns are stitched over every other warp yarn. The harness satin weave refers to the degree of stitching, e.g., one stitch over every eight warp yarns eight harness satin weave. The unbalanced weave contains a significantly greater number of warp yarns and is generally referred to according to the ratio of warp to fill yarns, e.g., six to one [2].

The final properties of the composite are controlled by the direction of the fiber layup. A warp aligned layup or 0° layup indicates all the warp fibers are aligned in the same direction. A balanced or 0-90° layup indicates that the fabric in every other ply is rotated by ninety degrees. An off axis layup refers to composites in which the fabrics are laid up at angles off the major directions, e.g., a +/-45° ply.

The processing step after fabric layup is the matrix formation. Forming a matrix with polymeric precursors will yield a polymeric precursor processing composite with two distinct sides, the bag and mold. The carbon fabric is laid up on an open mold and, in processing, the mold is placed in a plastic impregnation bag. A

vacuum is applied to this bag and then the fabric is impregnated with the precursor. The side against the mold has a smooth texture of the mold. The bag side is not as smooth because the composite surface is not restrained by the bag. These differences may influence mechanical test results.

After precursor impregnation are the cure and carbonization. The cure crosslinks and stabilizes the polymer. The carbonization cycle decomposes the polymer to a carbon char at high temperature and controlled atmosphere. Several cycles of impregnation and carbonization are required to produce a composite with significant integrity.

Another method to densify the composite is a CVD deposition of pyrolitic graphite to the matrix. This method requires heating the layup to high temperatures and passing a carbon containing gas through the fibers [1]. The carbon is deposited to the matrix from this gas.

## Oxidation of Carbon

The oxidation of carbon and graphite has been analyzed by a number of researchers [10-14], and some with a particular reference to c/c [15-17]. The oxidation of carbon is influenced by porosity, impurity content and crystallinity [11-14]. This may explain why researchers report different temperatures at which carbon oxidation exceeds one weight percent per twenty-four hours from 570°F (300°C) [13] to 840°F (450°C) [14]. However, temperature is the greatest factor in determining the rate of carbon oxidation [13,14]. The reaction rate below 1110°F (600°C) is controlled by the reaction of

active sites on or below the surface [10,12]. These sites include dislocations, basal plane edges, and impurities [19]. Between 1110°F (600°C) and 1470°F (800°C) the reaction rate is controlled by the transport of reaction gases, $O_2$, $CO_2$, and $H_2O$, to the active sites. Above 1470°F (800°C) the rate is controlled by the transport of reaction products across a stagnant film at the surface of the carbon. The reaction kinetics of c/c are similar to those just discussed for carbon [15,18].

The oxidation rate of carbon can be reduced by interfering with the operating oxidation mechanism [13]. Low temperature oxidation is controlled by the number of active sites, and these sites can be reduced by decreasing the porosity or chemically blocking the sites from oxidation. Most elements catalyze the oxidation reaction of carbon by acting as sites for oxidation [10, 11, 13, 17]. Therefore, these impurities must be minimized to decrease the rate. A few elements have an inhibiting effect on oxidation, such as boron, silicon, and phosphorus [11]. At higher temperatures the rate of oxidation can be reduced by decreasing the percent of reactants in the gas or reducing the flow rate across the specimen [14]. A coating will reduce the oxidation rate at all temperatures by effectively blocking the sites on the surface [13, 14], but cracks in the coating can serve as paths to oxidation sites.

The oxidation of carbon and c/c was examined by a few researchers [16, 20-22]. Han et al [16] analyzed the oxidation in a PAN fiber, pitch matrix c/c at the temperatures of 1110°F (600°C) and 1470°F (800°C). Preferential oxidation of the matrix over the fiber is

reported. Yasuda et al [15] examined the oxidation of PAN fiber, furfuryl alcohol matrix c/c, between the temperatures of 1200°F (650°C) and 1560°F (850°C). The oxidation attack is reported to begin at the fiber matrix interface and then progress successively to the grain boundaries in the matrix, the graphitic portions of the matrix, and then to the optically anisotropic regions of the matrix. The last part of the matrix to oxidize is the glassy region of the matrix. This preferential oxidation of the crystalline carbon over the glassy carbon is in conflict with the reports that glassy carbon oxidizes more readily than graphitic carbon [23].

## Stress Effects on Oxidation of Carbons

The effect of stress on the oxidation rate has been examined by a few researchers with contradictory results [24-27]. Stroud and Rummler measured the effect of stress on the oxidation rate of a coated RCC for space shuttle re-entry simulation tests. Examination at 2480°F (1360°C) [25] and stress level of 1.2 ksi (8.17 MPa) exhibited a six percent increase in mass loss over an unstressed specimen; at 1160°F (625°C) [24] and 1.0 ksi (6.8 MPa), no significant increase in mass loss occurred. Krefold et al [26] determined that a tensile stress on graphite increases the oxidation rate significantly in argon with small amounts of water vapor at 1830°F (1000°C). Thrower and Marx [27] conducted a similar experiment using compressive stresses. An effect on the oxidation rate was not found.

The effect of oxidation on the degradation of c/c mechanical properties was examined by Zhao et al [28]. The c/c examined was a

semirandom chopped PAN fiber with phenol, furfural resin char and CVD densification. The oxidation tests were conducted at 1110°F (600°C) in flowing air. Catastrophic effects on the mechanical properties occurred, e.g., for a twenty percent weight loss, Young's modulus decreased by 75% and flexure strength by 64%. The volume of the composite did not appreciably change with a 20% mass loss, indicating that oxidation occurred internally.

## Oxidation Protection of Carbon/Carbon

Numerous oxidation resistant coating and coating methods have been attempted for c/c. Coating systems with various carbides, nitrides, silicides, borides, and metals have been applied to c/c substrate with pack cementation, CVD, plasma spray, sputtering, and electro-deposition methods [2]. Many coating systems are unsuccessful because the mismatch of the thermal expansion coefficients causes coating failures. Cooling from the coating deposition temperature induces tensile strains in the coating because the thermal expansion of the c/c is less than that of the coating [29]. Ceramic coatings respond to this strain by cracking, leading to the oxidation of the substrate. Platinum and other ductile metal have been tried in an attempt to overcome this brittle failure mechanism, but failures have occurred with pinhole oxidation [30]. Room temperature deposition of coatings has also been attempted to avoid the tensile strains and cracks, but these coatings lacked sufficient adherence to the substrate.

Some ceramic materials are good candidates for coating c/c, but their success depends on their ability to close or seal the cracks at temperatures below 800°F (425°C), the temperature for the initial oxidation of carbon. The cracks in the coating are closed with thermal expansion forces on heating the composite. The temperature where the cracks close is called the crack closing temperature. If the coating system behaves perfectly elastically, this temperature is the coating deposition temperature. This assumption may not be valid for the c/c system because the substrate has low shear strength. With this low strength the c/c could accommodate some of the thermal expansion strains with plastic deformation. Plastic strains in the substrate reduce the amount of thermal strain recovery and subsequently reduce the crack closing temperature. This temperature may be reduced by application of a slurry of ceramic powders to the coating. These powders fill the cracks and decrease the width of the crack. A smaller crack width reduces the amount of strain recovery and subsequently reduces the crack closing temperature.

A coating system with a silicon base seals the cracks with a glassy layer. This coating system operates because the glass flows into the cracks to block the oxidation. The glass layer is formed by the oxidation of the silicon based coating. The melting temperature of silica is high and is lowered by applying glass modifiers as an overlay. The activation of the glass fluidity depends on the chemistry of the glass and a successful overlay activates around 1400°F (760°C). Other glass compositions activate at lower temperatures, but at the expense of higher temperature protection.

The lower temperature activated glasses are too fluid at the higher temperature and vaporize or flow off the coating. Therefore, the use of the higher activated glass is necessary, and an oxidation window exists between 800° and 1400°F (425° and 760°C).

Another oxidation protection method involves chemically inhibiting the oxidation of the c/c substrate. Elements that inhibit the oxidation of carbon are silicon, phosphorus and boron. Han et al [16] found that silicon carbide was an effective inhibitor up to 1110°F (600°C). McKee et al [22] examined the effects of phosphorus compounds on the oxidation rate between 1110°F (600°C) and 1560°F (850°C). The rates were different by an order of magnitude between the treated and untreated materials, but the apparent activation energies for oxidation were the same. This indicates a lower number of oxidation sites in the inhibited material with no change in the oxidation mechanism. Zhao et al [28] employed phosphorus as an oxidation inhibitor in c/c for tests at 1110°F (600°C) but did not report on the oxidation characteristics. The effectiveness of the phosphorus compound at inhibiting c/c above 1650°F (900°C) is questionable. The oxidation tests conducted by McKee [22] at a constant rising temperature found a 10% oxidation weight loss for a phosphorus inhibited material in the temperature range of 1650°F (900°C) to 1830°F (1000°C).

The inhibition of c/c oxidation with boron was examined by a number of researchers [20, 21]. McKee determined that a borate additive was effective at retarding the oxidation up to 1830°F (1000°C). Above this temperature, it was less effective because of

the volatility of borate glasses. Ehrburger et al [21] found that boron oxide in both small and large amounts effectively decreased the oxidation rate. This testing was conducted at temperatures below 1520°F (827°C) to avoid any possible loss of the boron oxide inhibitor through volatilization. Small amounts of boron oxide acted to block oxidation sites; large amounts acted as a diffusion barrier [21].

Future oxidation protection systems for c/c will incorporate both a coating and an inhibitor. This could yield the best properties because the glass overlay can seal the cracks in the coating on cool down until the glass becomes too viscous to flow. The inhibitor is active after the glass is ineffective to block oxidation. The largest concern will be the loss of the inhibitor because of volatility. However, a coating may reduce the loss of inhibitor.

## Mechanical Testing of Carbon/Carbon in Flexure

The mechanical properties of tensile, compression, and shear strengths and the modulus of c/c are a concern for designers of c/c components. The high temperature test methods have been developed for a vacuum environment [31]. The effect of an oxidizing environment on the strengths is a great concern. Tensile tests of high temperature composites in an oxidizing atmosphere are difficult to conduct because of the problems with gripping [32]. Bend testing is a method of determining the strength and overcoming the gripping problem. However, the analysis of the results is more complicated. Tensile, compressive, and shear stresses develop during a flexural test, and a pure stress state is required for accurate property measurements. A

discussion of the advantages and disadvantages of the flexure test method, particularly for brittle materials, is found in a number of reports [33, 34].

Flexure tests on coated c/c were conducted by researchers [2, 31, 33]; a few of these reports are reviewed here. Quinn and Stiglich [35] conducted flexural tests on a high modulus, coated c/c at room and elevated temperatures in air. The flexural strengths were not reported but relative flexural loads for these c/c materials showed a higher flexural strength for coated specimens compared to uncoated specimens. The flexural failure loads increased from room temperature to 2400°F. Two crosshead displacement velocities, 0.02 and 0.005 inches per minute, were employed in the flexure tests with no apparent affect on the strength of the composite.

Vought Corporation conducted mechanical tests on RCC material with a proprietary diffusion coating of silicon carbide and examined the effect of temperatures on the mechanical properties [36]. The data were presented in graphical form and the results were not summarized. The deflection for the modulus calculation was measured at two-thirds of the failure load. The modulus of a 19 ply RCC decreased from 2.35 to 2.15 Msi from room temperature to 500°F and then increased with temperature to 2.70 Msi at 2500°F (1370°C). The flexure strength decreased from the room temperature value to 8.0 ksi (55 MPa) at 1000°F (538°C) and increased to 9.0 ksi (62 MPa) at 2500°F (1370°C).

The application of mechanical loads to a silicon carbide coated c/c can cause the formation of cracks in the coating. An oxidation

pathway is opened by these cracks if the glass overlay does not seal the cracks. The glass overlay will be ineffective if the glass is too viscous to flow into the cracks or the cracks are too large for the glass to fill. The ability of coating to seal the cracks has been examined in a stress rupture tests [35,37]. Quinn and Stiglich [35] conducted stress rupture testing on eleven silicon carbide coated, high modulus, c/c specimens at the temperatures of 1830°, 2190°, and 2370°F (1000°, 1200°, and 1300°C) with significant scatter in the results. Most of the specimens that failed in the stress rupture test failed within two hours, while others at the same or greater normalized loads survived over a thousand hours. This inconsistency of failure times was experienced on a silicon carbide pack cementation coatings on high modulus materials by another researcher [37]. Static fatigue tests of monolithic ceramics exhibited a similar failure distribution [38]. The possibility of a stress rupture limit is indicated [35] but an insufficient number of tests were conducted. The combined loading and oxidation tests at 1600° and 2000°F (871° and 1093°C) are examined in a report [39]. Failures are not reported but permanent deformation was observed after four hours of testing.

Carbon/carbon composites retain their mechanical integrity to high temperatures and therefore, have potential in aeropropulsion applications. The good thermal qualities of c/c have already been employed in the space shuttle leading edges. Further implementation of c/c is restricted by the absence of inherent oxidation resistance and expensive fabrication procedures. The fabrication expense results from long process times to form the matrix by either CVD deposition of

carbon or charring of an organic precursor. The expense of c/c becomes minor, if a successful oxidation protection system is found. Oxidation of c/c occurs significantly above 800°F (425°C) and is reduced by a surface coating or impregnating the c/c with chemicals that inhibit carbon oxidation. Many coating systems have been attempted on c/c and have failed because thermal expansion mismatch strains crack the coating. Silicon based coating can prevent this failure mode by the flow of a glass surface layer into cracks to block oxidation. This coating type is more successful at higher temperatures than lower temperatures. Mechanical loads can also crack the coating and allow the oxidation of c/c. This failure mode is examined in the stress rupture test. The present research employed the stress rupture test to examine the effects of stress on the ability of a silicon carbide coating to protect a low modulus c/c.

# PROCEDURE AND MATERIALS

## Experimental

The primary purpose of this research was the examination of the ability of silicon carbide coating on a low modulus c/c to maintain oxidation protection when mechanically loaded. The tests were conducted in fast fracture and stress rupture modes. Properties measured were the shear and flexural strengths, and density. The coating thickness was measured, and the coating was characterized by chemical analysis. Differences among the three coating batches and between the bag and mold sides were determined in the characterization segment. The mechanical tests on coated c/c were conducted at elevated temperatures of 1000°, 1500°, 2000°, and 2400°F (538°, 816°, 1093°, and 1316°C). Flexural strengths and moduli were determined in a four point bend test at each temperature. The stress rupture tests were conducted with the same test geometry as the flexure test and were statically loaded. The stress rupture tests were conducted in a one hundred hour time period because this is a goal for the implementation of c/c in aerospace applications. Times to failure in the stress rupture tests are reported at various stress levels for each test temperature.

## Materials

The two major components of c/c specimens in the test sequence are the substrate and coating. The low strength, low modulus substrate is composed of low modulus fibers and a charred polymeric

matrix. The coating is a silicon carbide conversion of the composite surfaces, plus an overlay of glass sealers. The processing procedures of the substrate and coating are proprietary to Hitco of Gardena, California; therefore, only limited details about the production are explained here.

The precursors to the c/c substrate are low modulus carbon fibers for reinforcement and a phenolic resin to form the matrix. The fibers are rayon based and the yarns are woven into a balanced eight harness satin weave. The fabric designation is G2206. The strength of the fiber is 100 ksi (690 MPa); the modulus is 6 Msi (4.1 GPa). Each yarn contains approximately 720 fibers. The phenolic resin is carbonized at elevated temperatures. The properties of the char depend on carbonization time and temperature, and are proprietary.

The fabrication of the c/c substrate involves layup, impregnation, carbonization, and cutting into specimens. Initially a panel is molded to the dimensions of 17 by 12 by 0.24 inches thick (44 x 21 x 0.6 cm.) during the layup procedure. The G2206 fabric is cut to size and nineteen plies are incorporated in the fabrication. All the warp fibers are aligned in the same direction, and the crossovers are nested. Nesting is accomplished by laying up the fabric so that the crossover side of each ply contacts the crossover side of the adjacent ply. A bleeder cloth is set on the exterior surface of the molded panel and absorbs excess resin during impregnation.

Impregnation and carbonization are the next fabrication steps. The mold and layup are bagged using standard composite fabrication procedures. The phenolic precursor is vacuum impregnated to form the

panel and cured prior to carbonization. The bleeder cloth is subsequently consumed in the carbonization cycle and impresses the texture of the cloth to the bag side of the composite.

The panel is cut into specimens after the first carbonization cycle. A one-quarter inch strip is cut from the edges of the panel to remove possible edge effects. The dimensions of the specimens cut from this panel are 7.75 inches long by 0.6 inches wide (20 x 1.5 cm). The specimen thickness is approximately 0.24 inches (0.6 cm). The 165 specimens for this test sequence are cut from nine panels. After the specimens are sectioned, two additional impregnation and carbonization cycles are conducted on the specimens to complete the processing.

The low modulus c/c substrate is coated with a pack cementation conversion to silicon carbide plus an overlay of glass sealers. Twenty-eight of the 165 specimens were not coated. This particular coating was developed by Vought Corporation for the ACC material and is moderately successful at preventing the oxidation of this substrate. The Vought designation for this coating is type one, mod one. This coating technology is licensed to Hitco, the fabricators of the specimens.

The cementation coating procedures require placing the specimens in a pack of powders in a controlled atmosphere furnace. The pack of powders consists of a blend of mostly inert aluminum oxide and silicon with minor additions of silicon carbide and boron oxide. The c/c substrate is packed in this powder and heated at a controlled rate. The outer surfaces of the specimen are converted to silicon carbide. A glass overlay is applied to the coating surfaces after the

cementation process and is based on the organometallic compound, tetra ethyl ortho silicate. Three coating batches were required to coat the 137 specimens in the test sequence. Two batches of 50 and one of 37 specimens may lead to inconsistencies in testing results. Therefore, all tests included at least one specimen from each coating batch.

## Procedure

The experimental test procedures are divided into three sections: the characterization, the flexure tests, and the elevated temperature stress rupture tests. The characterization was employed to distinguish any inherent differences among the three coating batches, and differences between the sides of the specimens. The room and elevated temperature flexure tests were conducted with similar procedures, and established the strengths at the test temperatures. The stress rupture tests were conducted with the same testing geometry as the flexural tests but with the specimen statically loaded at stress levels less than the strength. The detail procedures for each test are presented in Appendix A.

## Characterization

The physical properties of density and coating thickness are useful in distinguishing differences between coating batches and specimen sides. The density of the coating and substrate is determined by a wax immersion technique for porous material [40]. The substrate density was determined with four coupons, 0.6 x 0.6 x 0.24 inches (1.5 x 1.5 x 0.6 mm), which were cut from three uncoated flexural specimens. Each specimen originates from different panels.

The density of the coating was measured by cutting coupons from both the bag and mold sides. These coupons are prepared by procedures explained in Appendix A. Four coating coupons were used for density measurements, two each from the bag and mold sides. The density of the coating and substrate are recorded in Tables B and C of Appendix B.

The thickness of the coating was measured at ten equidistant positions on a micrograph with a magnification of 50x. The thickness of the glass overlay was measured simultaneously. The mean, standard deviation, maximum and minimum values of thickness are reported for each coating batch with bag, mold, and edge sides. One micrograph was made with the warp yarns running parallel to the coating and another with fill yarns parallel to the coating. The edge micrographs were similar except that the fibers were perpendicular to the edge coating. The coating thickness values are recorded in Table D of Appendix B.

Mass chromotography and x-ray diffraction were used to indicate differences between coating batches and between the sides of the specimen. The chromotography techniques yielded an elemental analysis of the coating; the x-ray diffraction determined the crystallographic phases of the coating. The chromotography was employed for analysis of coating and ash on each side of a specimen from each coating batch. X-ray diffraction phase analysis of the coating was done on the bag and mold side from each coating batch. The results of this analysis are recorded in Tables E, F, and G of Appendix B.

The x-ray radiography shows differences between batches and internal defects within a specimen, such as delamination or

deleterious coating penetration. The radiograph is a record of the initial specimen condition. Radiographs were taken parallel and perpendicular to the plane of the specimens.

## Mechanical Testing

Flexure and shear test established the base line room temperature properties. The properties were measured with a four point bend fixture of stainless steel. The load span is one inch (2.5 cm) and the support span was varied to yield either a flexure or shear failure. The longer span of 6 1/8 inches (15.5 cm) yielded in a flexural mode and the shorter span of 1 1/2 inches (13.8 cm) failed in shear. The cross head deflection rate was 0.05 inches per minute (0.13 cm/min.). The load deflection curve was recorded on a strip chart recorder. The deflection was stopped when the load dropped off significantly. Strengths were calculated at the maximum load. The elastic modulus was determined at the deflection corresponding to one half of the maximum load. This deflection was corrected for the compliance of the test frame. The strength and modulus are reported for six coated specimens and eight uncoated specimens in Appendix B, Tables H and I.

A sintered alpha silicon carbide fixture was employed for testing the coated c/c specimens. The fixture had the same test geometry as the room temperature four point bend fixture. The tests were conducted in an Applied Test System (ATS) silicon carbide resistance furnace, using an Instron universal test frame to apply the load. The specimen and fixture were aligned and bonded with an adhesive

before being placed in the load train. The furnace was equilibrated at test temperature for one hour before testing. The flexural strength and proportional limit were calculated and are recorded in Tables L to O in Appendix B. The modulus was calculated with the method described in the room temperature tests.

## Stress Rupture Testing

The stress rupture tests of coated specimens were conducted at the same temperature and test geometries as the elevated temperature flexure tests. An ATS compression-creep test frame was employed to apply direct weight loading to the specimen. A three point extensometer with a linear variable differential transformer measured the relative deflection, and the data acquisition system calculated the strain. This test was conducted with procedures that are similar to the flexure test. The specimen was bonded to the test fixture and then placed in the load train. The specimen was equilibrated at temperature for one hour before the load was applied. The extensometer was brought into contact with the specimen prior to loading. The test lasted for 100 hours or to failure. This duration was chosen because 100 hours is an implementation goal for coated c/c in aerospace applications.

## RESULTS AND DISCUSSION

### Characterization

The density of the c/c substrate is 1.38 grams/ml; that of the coating is 2.63 grams/ml. The results for specimens from each coating batch are presented in Tables B and C of Appendix B. Significant density differences do not occur among the three batches or between the bag and mold sides of the coating. The maximum density difference among the three coating batches is less than 4%.

The average coating thickness for the three coating batches was 0.014 inches (0.035 cm.) on the ply side of the composite and 0.030 inches (0.075 cm.) on the edge of the composite. The coating thicknesses on the bag and the mold sides were similar within the same specimen and are averaged in Table I. A detailed summary of the coating thicknesses is listed in Table C on Appendix B. The thickness of a specimen from coating batch 1 was 33% greater than the thickness of one from coating batch 2 and 23% greater than one from batch 0.

The average thickness of the specimen from coating batch 1 does not indicate that this coating batch is thicker than the other two because thickness measurement of another specimen from coating batch 1 and a statistical test indicate otherwise. The average thickness of another specimen from coating batch 1 was 0.013 inches (0.033 cm.) which is similar to the other batches. A two tailed Z-test on the thickness data of batch 1 and 2 had a Z value of 0.53, which suggests that differences between the two coating batches are insignificant.

TABLE I

Coating Thickness Summary

| Coating Batch Number | Coating Thickness on ply in. | cm. | Standard Deviation of Coating Thickness | | Coating Thickness on edge in. | cm. |
|---|---|---|---|---|---|---|
| 0 | 0.013 | 0.033 | 0.003 | 0.008 | 0.032 | 0.081 |
| 1 | 0.016 | 0.041 | 0.004 | 0.010 | 0.029 | 0.074 |
| 2 | 0.012 | 0.030 | 0.002 | 0.005 | 0.028 | 0.071 |
| Average | 0.014 | 0.035 | | | 0.030 | 0.075 |

The chemical analysis of the coating and the ash of the substrate after coating are tabulated in Tables E and F of Appendix C. Silicon as $SiO_2$ is the major component and sodium as $Na_2O$ is the second most commonly occurring element. The percent of sodium in the ash is greater than in the coating. Sodium catalyzes the oxidation reaction of carbon [12] and has a significant impact on the corrosion of silicon carbide [41]. Sodium is a constituent of the tetra ethyl ortho silicate glass overlay and acts to reduce the viscosity. The other minor elements in the coating and ash are aluminum, boron, calcium, and iron. Aluminum and boron are constituents of the pack cementation process. The calcium and iron are present as impurities in the silicon carbide.

X-ray diffraction phase analysis of the coating reveals beta silicon carbide as a major phase. The x-ray diffraction peaks are tabulated in Table G of Appendix B and are ordered in decreasing peak intensity. The bag and mold sides in each of the coating batches exhibit the same peaks.

The results of the x-ray radiography indicate density or coating thickness differences by the intensities on the radiographs. The thinner or less dense areas of a material appear as brighter areas on the radiographs while denser or thicker areas are darker. The radiographs for the coated c/c are taken with the specimen parallel and perpendicular to the ply side of the composite. The radiographs reveal no delamination or coating penetration into the coated specimens. The variation of radiographic intensity that occurs among the specimens and within a specimen are exhibited in Figures 1 and 2. The intensity of the radiograph varies across the length of many specimens. These variations are attributed to variations in the coating thickness and not the density. The density and coating thickness measurements support this conclusion. The densities of the coatings vary less than 5.5% among the batches or within a specimen. The thickest coating measurements correspond to the darkest radiograph of the three specimens examined. This variation of the intensity observed in both parallel and perpendicular radiographs may originate with differences in the environment of the pack cementation furnace.

The perpendicular radiographs of the c/c specimens reveal that the specimens were distorted in all coating batches, as illustrated in Figure 2 for batch 2. The warpage of the specimens is attributed to the residual stresses originating from the coating process. The uncoated specimens are flat. The stress is developed as a result of the thermal expansion mismatch between the coating and substrate. The substrate is low modulus and consequently is easily deformed at low stress levels.

The radiography shows texture differences between the specimens from panels 8 and 11 than those from other panels. The texture in the radiograph of panels 8 and 11 consists of small rounded circles with a close ordered pattern. The radiographs of the other panels exhibit larger circles with a greater distance between the circles. Both textures are exhibited in Figure 1.

The perpendicular radiographs for specimens show differences between panels. Most specimens have a dark line about the centerline of the specimen as observed in Figure 2. This line runs the length of the specimen in the radiograph and is assumed to be a higher density area. The specimens from panel 8 do not show this line. Panel 11 has a lighter line about the centerline, and this may indicate an area of lower density.

## Mechanical Tests

The final and most significant results in this study are the mechanical testing of coated and uncoated c/c samples. Flexure and shear tests measured the room temperature strength and modulus in four point bending. The strength ranges from 12.8 to 14.1 ksi (88 to 97 MPa) with an average of 13.6 ksi (94 MPa). Figure 3 is a typical room temperature load deflection curve of uncoated c/c. The proportional limit is not apparent in the load deflection curve. Therefore, the modulus is calculated with the deflection corresponding to one half the maximum load. The average modulus value is 2.3 Msi (16 GPa). The measured moduli vary from 2.0 to 2.7 Msi (14 to 19 GPa). The mechanical properties for each uncoated specimen are recorded in Table

H of Appendix B. The room temperature flexure specimens failed with a substantial load decrease. The fractures were initiated on the tension side and then propagated to the compression side. Two specimens from panels 3 and 6 fractured into two separate pieces. The remaining specimens failed almost as catastrophically.

Six low modulus coated c/c specimens yielded an average strength of 12.8 ksi (88 MPa) and a range of values from 12.1 to 13.5 ksi (83 to 93 MPa) at room temperature. A typical load deflection curve for a coated c/c at room temperature is plotted in Figure 4. A proportional limit is not observed so the modulus is calculated from the deflection at one half the maximum load. The data for these flexural tests on the coated c/c are recorded in Table I of Appendix B. The average modulus for the coated specimen at room temperature is 3.0 Msi (20 GPa) with the values ranging from 2.7 to 3.4 Msi (19 to 23 GPa).

The flexural test characteristics on coated c/c are discussed with regard to the load deflection curve, deflection to failure, and type of failure. All of the specimens failed on the tension side of the maximum stress zone between the load points. The failure was a single crack across the width of the specimen that did not propagate to the compression side except in one specimen. Most retained some load carrying capability. One specimen from panel 6 failed catastrophically into 2 pieces while the other one from the same panel did not. The amount of deflection to maximum load experienced by these c/c flexure tests has an average value of 0.18 inches (0.46 cm). These deflection values were not correlated with any of the mechanical properties.

The typical load-deflection curves for the coated and uncoated c/c specimens is shown in Figures 3 and 4. The failure load decrease is greater for the uncoated material than the coated. The load-deflection curve is rounded near the maximum load for the coated specimens and indicates that additional failure mechanisms are operating. This rounding off may indicate debonding.

The shear strength of the c/c material is apparently so high that shear failures could not be obtained on the uncoated or coated material. When the specimens were tested in short support span, the shear stress failures occurred in surface crushing rather than in shear. Based on these observations it is believed that the shear strengths in the coated and uncoated conditions are greater than 2600 and 2400 psi (18 and 17 MPa) respectively. The data for the shear tests are listed in Tables J and K of Appendix B for uncoated and coated c/c respectively.

## Elevated Temperature Flexural Testing

Results of the flexural test that was conducted at room temperature and 1000°, 1500°, 2000°, and 2400°F (538°, 816°, 1093°, 1316°C) are summarized in Table II. The results on the individual tests are listed in Tables L, M, N, and O in Appendix B. It is noted that the flexural strength first decreases slightly then increases with increasing temperature. The proportional limit is observed at an elevated temperature and increases with increasing temperature. The proportional limit is considered as the point where the load versus deflection curve deviates from linearity. The modulus of

elasticity is taken as the initial slope of this curve and is significantly higher at elevated temperatures compared to the room temperature value.

TABLE II

Summary of Flexural Test Data

| Test Temperature °F | Test Temperature °C | Flexural Strength ksi | Flexural Strength MPa | Proportional Limit ksi | Proportional Limit MPa | Flexural Modulus Msi | Flexural Modulus GPa |
|---|---|---|---|---|---|---|---|
| RT | RT | 12.6 | 87 | - | - | 3.0 | 21 |
| 1000 | 538 | 12.4 | 85 | 4.0 | 28 | 6.0 | 41 |
| 1500 | 816 | 12.4 | 85 | 4.6 | 32 | 7.1 | 48 |
| 2000 | 1093 | 13.3 | 92 | 6.3 | 43 | 6.9 | 48 |
| 2400 | 1316 | 14.6 | 101 | 7.3 | 50 | 6.3 | 44 |

The influence of temperature on the mechanical strength of a low modulus, coated c/c composite has been plotted in Figure 5 with the data listed in Table II. The modulus of elasticity (as measured from the slope of the initial linear portion of the load-deflection curve) is plotted in Figure 6 with the data in Table II. The proportional limits are plotted in Figure 7 with the data in Table II.

The average flexure strength decreasesd 3% from its room temperature value, to the value at 1000°F, the average modulus of elasticity increased by 100%, and the proportional limit was first observed at this temperature. At 1500°F as compared to 1000°F, the average flexural strength remained the same, the elastic modulus increased by 17%, and the proportional limit increased by 14%. For the bend tests at 2000°F as compared to 1500°F, the average strength

increased 7%, the average modulus decreased by 1%, and the proportional limit increased by 37%. For the flexure at 2400°F as compared to the 2000°F, the average strength increased by 10%, the elastic modulus decreased by 7%, and the average proportional limit increased by 16%.

Three types of load versus deflection curves were observed during the flexure tests. The most commonly occurring curve is illustrated in Figure 8 and shows significant load decrease after the maximum load. The second type of curve, which is demonstrated in Figure 9, shows more rounding at peak loads than the other curves. The third type of curve shows only a small decrease in load when it falls off from the peak load, as indicated in Figure 10. The type of curve that occurred in each test is indicated in data tables in Appendix B.

All of the load-deflection curves at room temperature, 2000°, and 2400°F exhibited the rapid decrease in load from the maximum load illustrated in Figure 8. One of the curves at 1000°F exhibited a rounded portion at the maximum load as demonstrated in Figure 9. This was the only specimen to fail in this manner. Its behavior is attributed to the structure of the c/c composite and the occurrence of small internal cracking. The small decrease in load from the maximum load, shown by the load-deflection curve demonstrated in Figure 10, only occurred at 1500°F and is believed to be associated with the behavior of the coating.

When failure occurred on these specimens it followed two modes. In one case, the specimen broke completely through its cross section, and in the other case considerable internal cracking occurred but the

specimen remained intact. The initial fracture appears to have multiple cracks in the coating that are perpendicular to the major stress and strain axis. The failure cracks always occur on the tension side and eventually coalesce into a failure.

The composite separation of the flexure specimen into two pieces occurred with some specimens at all temperatures except at 1500° and 2400°F. At 1500° and 2400°F all of the fractures were of the partial type with some load carrying characteristics remaining. Tables O through R in Appendix B indicate the fracture modes of the individual specimens. All failures started on the tension side of the bend specimen. In the case of the complete separation fracture, the failure followed about a 30° angle from the vertical in transversing across the specimen. This indicated a stepwise type of fracture.

## Stress Rupture Testing

The results of the stress rupture tests that were conducted at the elevated temperatures of 1000°, 1500°, 2000°, and 2400°, (538°, 816°, 1093°, and 1316°C) indicate the existence of a stress rupture limit in the silicon carbide coated, low modulus c/c composites. The stress rupture limit is defined as the applied stress load to the c/c that will not cause failure of the specimens within 100 hours. The stress rupture limit increases with increasing temperature and is listed in Table III. The times to failure at stress levels above the stress rupture limit are listed in Table IV. Times to failure increased as the applied stress was decreased. The test data for each individual test is tabulated by temperature in Tables P, Q, R, and S of Appendix B.

TABLE III

Stress Rupture Summary
Stress Rupture Limit

| Temperature °F | Temperature °C | Stress Rupture Limit ksi | Stress Rupture Limit MPa |
|---|---|---|---|
| 1000 | 538 | 3.0 | 21 |
| 1500 | 816 | 6.3 | 44 |
| 2000 | 1093 | 7.9 | 54 |
| 2400 | 1316 | 9.2 | 62 |

TABLE IV

Stress Rupture Summary
Times to Failure

| | | | | Times to Failure (hours) Stress Levels ksi (MPa) | | |
|---|---|---|---|---|---|---|
| | | | | 6.5 (45) | 5 (34) | 3.2 (22) |
| 1000 | 538 | | | 7.3 | 12 | 39 |
| 1500 | 816 | 1. | ∠ | 26 | - | - |
| 2000 | 1093 | 2.1 | 4.0 | - | - | - |
| 2400 | 1316 | 1.5 | - | - | - | - |

- indicates no failure or not test conducted.

A specimen in the stress rupture test failed after the application of a static flexure stress. This stress cracked the coating and created a path for the oxidation of the substrate. The glass overlay flowed into the cracks, if the glass was fluid, and

blocked the oxidation path. A minimum stress level induced cracks in the coating that were too large for the glass layer for fill. Subsequently, the substrate was oxidized and the composite failed. This minimum stress level is just above the stress rupture limit.

Four types of specimen fracture occur during the stress rupture tests. Figure 11 is a photo of a single crack fracture which occurred at all temperatures and is characterized by one dominant crack in the coating in the high stress area. Figure 12 is an example of the second type of fracture, a split fracture, and is characterized by one major crack on one specimen edge and two separate cracks on the other edge. The coating between these two cracks frequently breaks off during handling. The third fracture type is shown in Figure 13 and is a ply shear fracture with multiple cracks in the coating. This fracture pattern has one major crack on the mold side of the coating and one crack through the thickness of the specimen. The mold side crack propagates through the thickness of the coating and then runs parallel to the mold side in a mode similar to shearing. This is illustrated in Figure 13. Figure 14 is an example of the fourth fracture type and is a wide fracture with multiple cracks in the coating. No major thickness crack is observed in this failure.

Significant scatter occurred in the stress rupture test data. The times to failure at a constant stress level and temperature varyed greatly and were not correlated with the number of cracks in the coating, initial strain rate, or fracture type. Some specimens failed in stress rupture while others do not fail at the same or greater stress level. The scatter of the failures and nonfailures is attributed to variations in the specimens.

The influence of temperature on the stress rupture limit of the silicon carbide coated, low modulus c/c has been plotted in Figure 15 from the data listed in Table III. The stress rupture limit at 1500°F is 100% greater than the value at 1000°F. The tests at 2000°F exhibit a 26% increase of the stress rupture limit compared to the value at 1500°F. The stress rupture limit at 2400°F is 18% greater than the value at 2000°F.

The influence of applied stress on the time to failure is plotted for the 1000°F stress rupture test in Figure 16 with data listed in Table P of Appendix C. This plot is similar in shape to the other temperature curves except for higher stress rupture limits and the occurance of failures beyond the 26 hours. Only one test at 1500°F failed in excess of 26 hours. This specimen failed in 58 hours and the strain was constant from the 8th hour to the 48th hour. The strain then increased and failure occurred within 10 hours after strain initiation. The longest length of a test at 2000°F that resulted in failure was 3.7 hours; at 2400°F, 2.2 hours for stress levels just above the stress rupture limit.

The influence of temperature on the time to failure at a constant stress has been plotted in Figure 17 with the data listed in Table IV at the stresses of 8.0 and 9.5 ksi (5.5 and 6.5 MPa). The time to failure with a 9.5 ksi load decreased by 50% with an increase in temperature to 1500°F from 1000°F. The failure time at 9.5 ksi is 30% greater at 2000°F compared to the 1500°F test. The time to failure is 30% less at 2400°F than the time at 2000°F. The increase in the time to failure at the 2000°F is attributed to a statistical variation.

One specimen at 2000°F and 9.5 ksi had a high failure time and influenced the average. The time to failure increase between 1500°F and 2000°F was not observed at the 8.0 ksi stress level and indicates that the increase at 9.5 ksi was not characteristic.

All of the fractures in the stress rupture test at 2400°F were a single crack fracture mode as seen in Figure 11. This fracture mode is observed at all temperatures and is the most frequently encountered at 2000°F. The split fracture mode is seen in Figure 12 and occured in the stress rupture tests at 1000, 1500 and 2000°F. Most of the 1500°F stress rupture test specimens fractured in this mode. The ply shear and the wide fracture modes were encountered only in the 1000°F stress rupture test and are seen in Figures 13 and 14. These modes are characterized by many cracks in the coating.

The oxidation of the composite in the stress rupture test is examined on random specimens. One failed stress rupture specimen from each test temperature was prepared for an optical examination along with a room temperature flexure specimen. These specimens were vacuum impregnated, cut longitudinally, and polished. These cross sections are presented in Figure 18 in ascending order by temperature, i.e. the room temperature specimen at the bottom and the 2400°F (1316°C) specimen at the top. The upper sample is at the bottom of this figure. The four oxidized samples have void areas under the coating. The 1000°F sample is different than the other higher temperature samples due to a depression area in the central portion of the composite. This area is believed to be evidence of internal oxidation which is the controlling oxidation mechanism. The oxidation of the

higher temperature specimens appears to occur by surface oxidation in a pore under a crack in the coating.

## Discussion

### Characterization

Some correlation of the mechanical properties to x-ray radiographic inspection are indicated. The differences between specimens from panels 8 and 11 and other panels are previously described. The specimen strength from these two panels are the lowest two values, 13.1 and 12.8 ksi (90 and 88 MPa), respectively. The moduli of these two panels are also the lowest values, 2.2 and 2.0 Msi (15 and 14 GPa). Removing these values from the calculations of the averages increases the average strength to 13.9 ksi (95 MPa) and the modulus to 2.4 Msi (16 GPa). The lower mechanical strength and modulus is observed at 1000° and 2400°F for the specimens from Panel 8. The strength and modulus of Panel 11 is among the highest at 2400°F. The effect of radiographic texture on the mechanical properties is inconclusive. The radiographic differences had no effect on the stress rupture test data.

### Flexural Testing

Results show a decrease of 6% in flexural strength for the coated compared to the uncoated specimens. Calculations based on the thickness of the coating compared to the specimen have been made to determine the cause of this different strength. The coating is approximately 12% of the specimen thickness and 10% of the width.

These calculations indicate that if the coatings were not bearing some of the load, the strength would decrease by 30%. This indicates that the coating is carrying some of the stresses in bending. In addition, the modulus of elasticity of the coating is somewhat higher than the value for the c/c material. This results in moving the neutral axis towards any side bearing a higher proportion of the stresses. Because of the presence of cracks in the coating that occur more readily on the tension side, the neutral axis moves toward the compression side. The cracks in the coating on the tension side lower the samples load carrying capability and produce higher stress in the composite material directly under the coating. Observations of this failure type show that the cracks occur in this region.

The behavior of the flexural strengths of the coated c/c composites with temperature is similar to results obtained on silicon carbide coated RCC-3 material by Vought [36]. The strength of a 19 ply RCC-3 is 14% greater than the value in this test sequence. The strength of the RCC-3 is reported to decrease first with temperature and then increase to 2% greater than the room temperature value at 2000°F. The strength increased further at higher temperatures. The proportional limit was not reported.

The strength decrease of a coated c/c from room temperature to 1000° and 1500°F (538° and 816°C) is insignificant as determined by a two sample t test at a 0.05 confidence level. This test also showed that the strength increases at 2000° and 2400° (1093° and 1316°C) were insignificant. The strength of the fiber is greater at temperatures above room temperatures [43].

The influence of the coating on the flexural strength and modulus is expected; however, the actual modulus increase is unexpectantly large. The elastic behavior of the uncoated, low modulus c/c with temperature is not reported in the literature. Information [2] on elastic properties of uncoated, high modulus materials indicates that the modulus is constant with temperature in an inert atmosphere. Also, the modulus of the fiber does not increase with temperature [42]. These two facts indicate that the coating must be dominating the load path at higher temperatures.

The modulus increase phenomena is also observed on the RCC-3 material, but the magnitude of the increase in the RCC-3 is less than the c/c examined in this test sequence. The modulus of the coated RCC-3 material in the flexural test increased with temperature. The modulus of the coated RCC-3 material increased 45% at 1000°F and 70% at 2000°F. The difference between the behavior of the two moduli is attributed to coating thickness differences. The coating thickness on the RCC-3 material is 0.006 inches (0.015 cm.) and is less than half the thickness of the coating in this test sequence.

The coating carried tensile and compressive stresses in the elevated temperature flexural test. In the room temperature flexural test the coating carried only compressive stress because of the presence of cracks as previously described. The coating carried tensile stress at elevated temperature because the cracks in the coating were closed by thermal expansion mismatch forces. The tensile stress in the coating is indicated by the proportional limit, the slope of the load-deflection curve, and the increase in the elastic

modulus. The proportional limit is attributed to the failure of the coating in tension and subsequently the shedding of all of the tensile stresses. The load is then carried by the substrate and the coating in compression. This load distribution is similar to the load distribution in the room temperature flexural test. The slope of the load-deflection curve above the proportional limit indicated this load distribution because this slope was similar to the room temperature slope. The modulus at elevated temperatures was more than double the room temperature value. The modulus of c/c is constant with temperature. Therefore, the additional load carrying capacity can only be attributed to the tensile loads in the coating.

The coating carried tensile loads because the cracks in the coating were closed by thermal expansion mismatch forces. The thermal expansion of the coating is greater than the thermal expansion of the composite. This system yields a temperature known as the crack closing temperature. All the cracks in the coating are closed by thermal expansion forces at this temperature. In a perfectly elastic system this temperature is the coating deposition temperature. The specimens in this sequence do not behave perfectly elastically because the crack closing temperature is less than 1000°F (538°C) while the coating is deposited in the temperature range of 2200° to 2400°F (1200° to 1300°C). The lower crack closing temperature is attributed to the overlay of glass sealers applied at room temperature. This slurry decreased the crack width and aided the healing of the cracks. Additional plastic deformation was believed to occur because of the warp character of the specimen as evidenced by the radiograph in

Figure 2. This deformation was part of the inelastic behavior that can decrease the crack closing temperature. Evidence of this deformation was not indicated by microscope investigation.

The modulus of the coating at elevated temperature was influenced by the thermal behavior and bonding within the coating. The modulus increased significantly from room to elevated temperatures. This increase is attributed to the coating carrying tensile loads. The weak links in the coating are the cracks in the coating. Healing of these cracks is required for the transfer load in the coating. The healing occurs by thermal mechanical closing of the cracks and bonding. At 1000°F (538°C) only compressive stresses and thermal energy assist the healing of the cracks. Above 1400°F (760°C) a liquid phase bonding mechanism improves the healing of the cracks and result in a higher moduli at 1500°F (816°C) and above. The decline of the modulus at 2400°F (1316°C) is attributed to the decrease in the modulus of the coating at that temperature.

The proportional limit of the c/c specimens increased with temperature because the amount of compressive stress in the coating increased with temperature. Compressive stress was induced in the coating with thermal expansion forces by heating a specimen to above the crack closing temperature. The amount of compressive stress in the coating is proportional to the temperature above the crack closing temperature. The initial loading in the flexural test decreased this compressive load in the coating before a tensile stress was induced in the coating. This compressive stress increased with temperature and required more load to overcome this stress.

Subsequently, the proportional limit increased with temperature. The proportional limit is believed to be influenced by other factors, but not as strongly.

## Stress Rupture Testing

The increase of the stress rupture limit with temperature increases is attributed to two factors: the fluidity of the glass overlay and compressive stress in the coating. The compressive stress in the coating increased with temperature increases as previously described for the proportional limit. The higher compressive stress increased the minimum load to cause a sufficiently large crack in the coating and allow the oxidation of the substrate. Subsequently, higher loads were employed at higher temperatures to obtain a stress rupture failure and stress rupture limit. A specimen failed in a stress rupture test because the glass layer flowed too slowly into the stress induced crack; consequently, the substrate oxidized. The fluidity of the glass increases with temperature. Therefore, the flow of the glass, to block the oxidation, improved with increasing temperature. This improved oxidation protection increased the stress rupture limit with increasing temperatures.

The results of this testing sequence indicate that this coating system is successful at preventing oxidation of the low modulus c/c. Compressive stress is induced in the coating upon heating and is desirable because the cracks in the coating are closed. The compressive stress arises from one or both of two mechanisms: the overlay of glass sealers at room temperature reduces the crack width, or plastic deformation within the composite accommodates the thermal

expansion mismatch strains. If the latter is the dominating mechanism then the coating retains the compressive stress on thermal cycling and the coating is a successful oxidation barrier. If the first mechanism is dominating, then with thermal cycling cracks are formed in the coating and the coating is an unsuccessful oxidation barrier. The thermal cycling testing is important because this environment is experienced in propulsion systems. Future examinations will combine stress rupture and thermal cycling tests to examine both of these affects on a coating ability to prevent oxidation.

## CONCLUSIONS

The following conclusions are based on the results obtained in this work on a silicon carbide coated, low modulus carbon/carbon (c/c) composite.

1) The stress rupture data indicates the existence of a stress rupture limit at each temperature; below this limit, failure does not occur. The stress rupture limit increases 100% between 1000° and 1500°F. This increase is attributed to the activation of glass sealers above 1400°F to block oxidation. The stress rupture limit increase is linear from 1500° to 2400°F for a total of 48%. Some tests above the stress rupture limit did not fail in the 100 hour time limit while others failed at equal or lower calculated stresses. The scatter of the failures is attributed to variations in the material. The scatter of times to failure is greater at lower temperature and stresses; this behavior is attributed to the number of oxidation sites and cracks in the coating.

2) The flexural strength at elevated temperature compared to room temperature initially decreases and at 2400°F increases to 15% greater than the room temperature strength . A proportional limit is not observed at room temperatures but occurs at elevated temperatures. This proportional limit increases with increasing temperature. The elastic modulus of the composite at room temperature is 30% higher for the coated than the uncoated specimens. The modulus of elasticity increases by greater than 100% at 1000°F compared to the room temperature value. Further

smaller increases are observed with increasing temperature until it decreases at the highest temperature, 2400°F.

3) The radiographic examination of the coated c/c revealed two different textures. The mechanical properties are not significantly different between the specimens of the two types of textures. The chemical and physical characterization of the composite did not yield significant differences among the coating batches and between the bag and mold side of the composite.

## REFERENCES


1. D. L. Schmidt, "Carbon/Carbon Composites", SAMPE Journal, 8 [3], pp. 9-19, 1972.
2. T. E. Schmid, "Oxidation Resistant Carbon/Carbon Composites for Turbine Engine AFT Sections", AFWAL-TR-82-4159, pp. 74-77, 105, 168, 1982.
3. A. J. Klein, "Carbon/Carbon Composites", Advanced Materials and Processes, 130 [5], pp. 64-68, 1986.
4. E. Fitzer, "The Future of Carbon-Carbon Composites", Carbon 25 [2], pp. 163-190, 1987.
5. H. M. Stoller, B. L. Butler, J. D. Theis, and M. L. Lieberman, "Carbon Fiber Reinforced Carbon Matrix Composites", in Composites: State of the Art, Proceedings AIME Fall Meeting, 1971, J. W. Weeton, and E. Scala, eds., pp. 69-136, 1974.
6. J. W. Warren and C. D. Coulbert, "An Introduction to Carbon Composite Materials", Super-Temp Company; Santa Fe Springs, CA. Report, pp. 3-14, 1971.
7. J. B. Donnet and R. C. Bansal, Carbon Fibers, Marcel Dekker, Inc. New York, pp. 7-10, 1982.
8. Ibid, Ref. 7, p. 226.
9. M. R. Piggot, Load-Bearing Fibre Composites, Pergamon Press, New York, p. 59, 1980.
10. H. W. Chang and S. K. Rhee, "Oxidation of Carbon Derived from Phenolic Resin", Carbon, 16 [1], pp. 17-20, 1978.

11. F. M. Lang and P. Magnier, "Action of Oxygen and Carbon Dioxide Above 100 Millibars on "Pure" Carbon", in Chemistry and Physics of Carbon, P. L. Walker ed., Marcel Dekker, New York, pp. 121-209, 1968.

12. W. S. Horton, "Oxidation of Pyrolytic Graphite" in Proceedings of the Fifth Conference on Carbon, Vol. 2, MacMillan Company, New York, pp. 223-241, 1963.

13. T. J. Clark, R. E. Woodley, and D. R. DeHalas, "Gas-Graphite Systems", in Nuclear Graphite, R. E. Nightengale, ed., Academic Press, New York, pp. 387-441, 1962.

14. A. J. Kennedy, "Initial Assessment of Graphite as a Structural Material in Conditions of High Thermal Flux", NATO, 1960.

15. E. Yasuda, S. Kimura, and Y. Shibusa, "Oxidation Behavior of Carbon Fiber/Glassy Carbon Composite", Transactions of the Japanese Society of Composite Materials, 6 [1], pp. 14-23, 1980.

16. K. H. Han, H. Ono, K. S. Goto, and G. R. St. Pierre, "Rate of Oxidation Carbon Fiber/Carbon Matrix Composites with an Anti Oxidation at High Temperature", Journal of the Electrochemical Society: Solid-State Science and Technology, 134 [4], pp. 1003-1009, 1987.

17. H. W. Chang and R. M. Rusnak, "Oxidation Behavior of Carbon/Carbon Composites", Carbon, 17 [5], pp. 407-410, 1979.

18. C. L. Mantel, Carbon and Graphite Handbook, Interscience Publishers, New York, p. 350, 1968.

19. G. R. Hennig, "Surface Oxides on Graphite Single Crystal", Proceedings of the Fifth Conference on Carbon, Vol. 1, MacMillan Company, New York, pp. 143-146, 1962.

20. D. W. McKee, "Borate Treatment of Carbon Fibers and Carbon/Carbon Composites for Improved Oxidation Resistance", Carbon, 24 [6], pp. 737-741, 1986.

21. P. Ehrburger, P. Baranne, and J. LaHaye, "Inhibition of Oxidation of c/c Composites by Boron Oxide", Carbon, 24 [4], pp. 495-99, 1986.

22. D. W. McKee, C. L. Spiro, and E. J. Lamby, "The Inhibition of Graphite Oxidation by Phosphorus Additives", Carbon, 22 [3], pp. 285-290, 1984.

23. J. B. Donnet and A. Voet, Carbon Black, Marcel Dekker, New York, p. 147, 1976.

24. C. W. Stroud and D. R. Rummler, "Mass Loss of a TEOS-Coated Reinforced Carbon/Carbon Composite Subjected to a Simulated Shuttle Entry Environment", NASA TM 81799, 1980.

25. C. W. Stroud and D. R. Rummler, "Mass Loss of TEOS-Coated RCC Subjected to the Environment at the Shuttle Wing Leading Edge", NASA TM 83203, 1981.

26. R. Krefold, G. Linkenheil, P. Glaud and W. Karcher, Carbon '72, Baden-Baden, p. 216, 1972.

27. D. R. Marx and P. A. Thrower, "An Investigation of Stress Effects on Graphite Oxidation", Carbon, 21 [4], pp. 451-459, 1983.

28. J. K. Zhao, R. C. Bradt, and P. L. Walker, "Effect of Air Oxidation at 873°K on The Mechanical Properties of a Carbon/Carbon Composite", Carbon, 23 [1], pp. 9-13, 1985.

29. D. L. Chang and L. Rubin, "Mechanical and Thermomechanical Responses of Silicon Carbide Coated Composites", SD-TR-83-33, 1983, p. 33.

30. R. Keiser, "Oxidation Protection for High Strength Carbon/Carbon Composites", AFWAL-TR-82-4060, 1982, p. 149.

31. C. D. Pears, H. S. Starrett, G. W. Driggers and D. L. VanWagner, "Test Methods for High Temperature Material Characterization", AFML-TR-79-4002, p. 335, 1979.

32. J. Z. Gyekenyesi, and J. H. Hemann, "High Temperature Tensile Testing of Ceramic Composites", NASA CR in publication, 1987.

33. J. S. Evangelides, R. A. Meyer and J. E. Zimmer, "Investigation of the Properties of Carbon/Carbon Composites and Their Relationship to Non-destructive Test Measurements", AFML-TR-70-213, 1971.

34. Y. M. Tarnopolskii and T. Kincis, "Methods of Static Testing for Composites" in Failure Mechanics of Composites, eds. G. C. Sih and A. M. Skudra. Elsevier Science Publishers B. V. Amsterdam, Netherlands, 1985, pp. 266-267.

35. G. D. Quinn and J. J. Stiglich, "Mechanical Testing of Coated Carbon/Carbon Composite at Elevated Temperature in Air", MTL TR 86-15, 1986.

36. T. W. Smith, et al., "Leading Edge Structural Subsystem Mechanical Design Allowable", Vol. II, Vought Corporation report 221RP00439, 1976.

37. K. Tossi, Personal Communication.

38. G. D. Quinn, "Review of Static Fatigue in Silicon Nitride and Silicon Carbide", Ceramic Engineering and Science Proceedings, 3, 1-2, pp. 77-98, 1982.

39. J. Fullerton, T. E. Schmid, and R. E. Warburton, "Carbon/Carbon Composites for Advanced Turbine Exhaust Nozzles", AFWAL TR-80-2104, 1980, p. 54.

40. "Bulk Density of Porous Refractories by Wax Immersion", C914, Annual Book of ASTM Standards, Section 15, Volume 15.01.

41. J. L. Smialek and N. S. Jacobson, "Mechanism of Strength Degradation For Hot Corrosion of α-SiC," Journal of the American Ceramic Society, 69 [10], pp. 741-752, 1986.

42. Personal Communication Greg A. Underwood, Hercules Aerospace Company, Magna, Utah.

43. R. M. Gill, Carbon Fibers in Composite Materials, The Plastic Institute, Butterworth and Co., Ltd., 1972, p. 72.

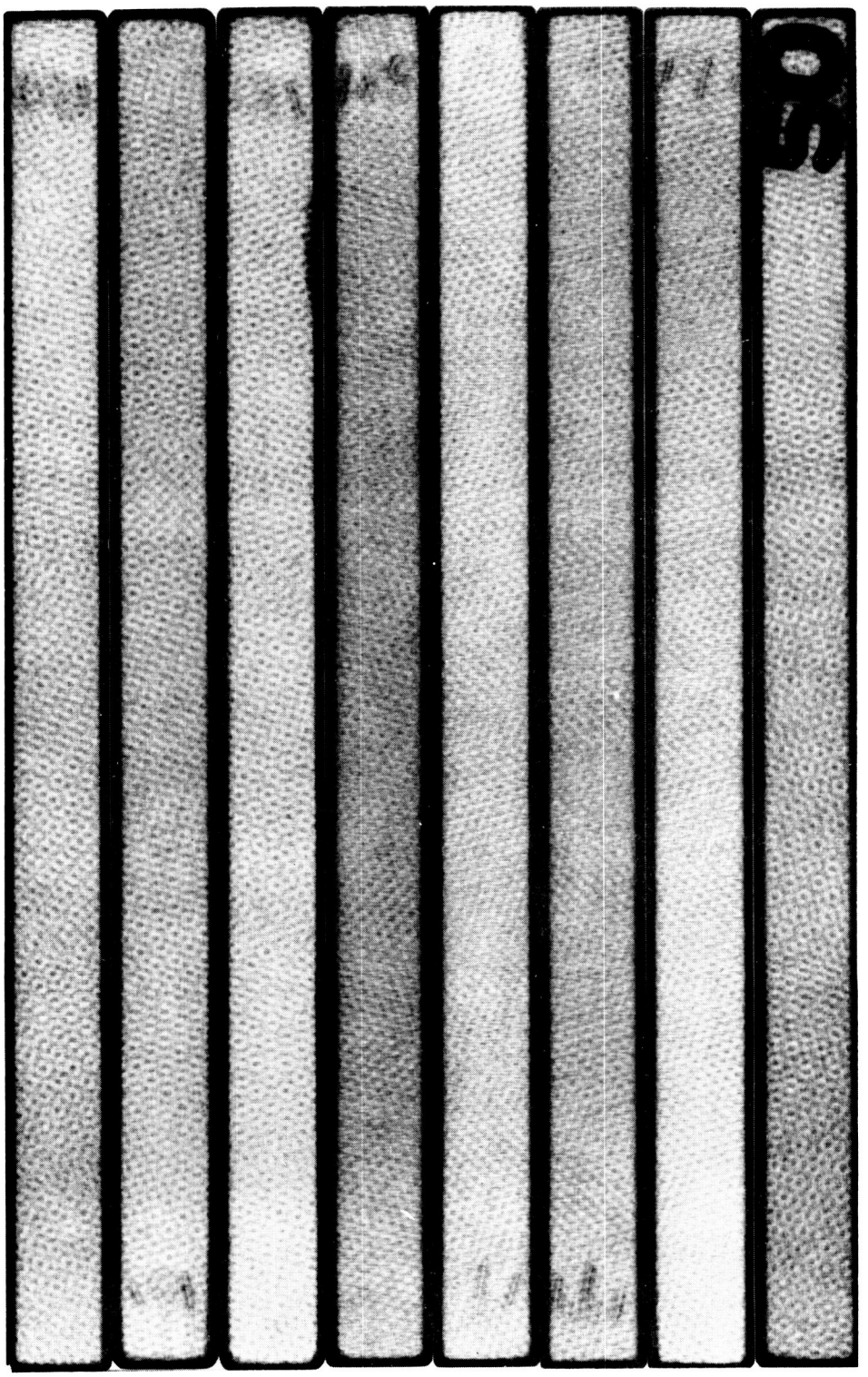

Figure 1. Typical radiograph of coated c/c perpendicular to the plies for the specimens 2-43 to 2-50.

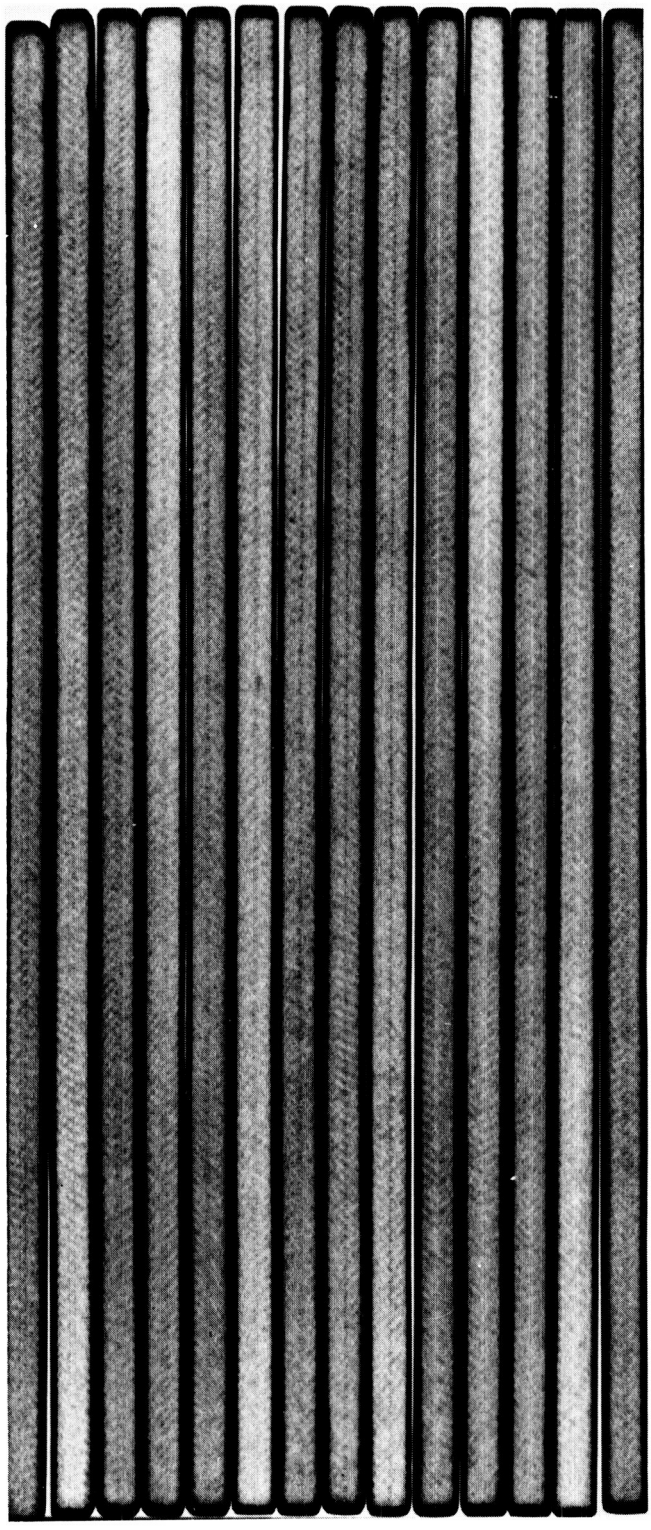

Figure 2. Typical radiograph of coated c/c parallel to the plies for the specimens 2-37 to 2-50.

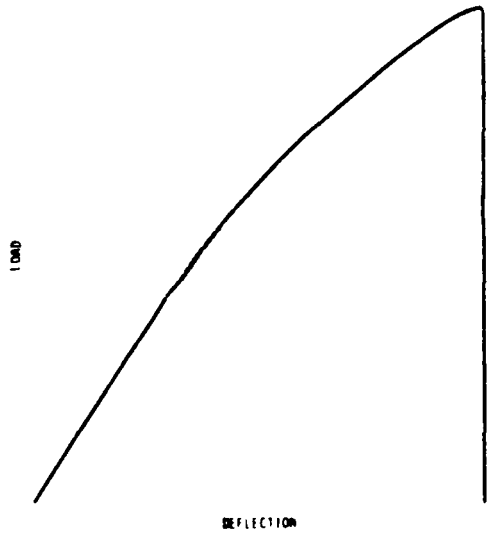


Figure 3. Typical load-deflection curve of an uncoated carbon/carbon composite in four point flexure at room temperature.

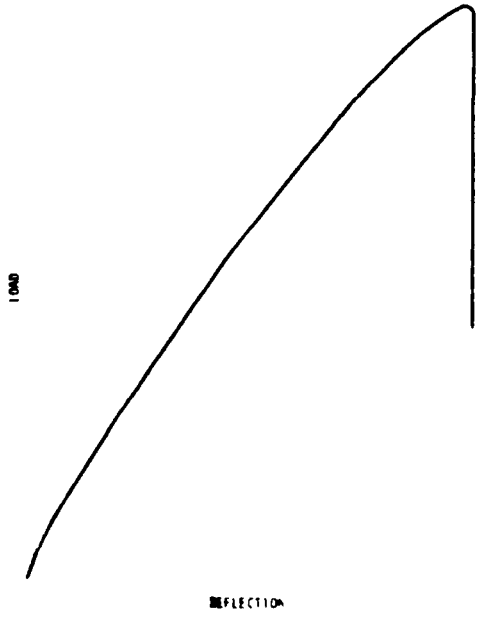


Figure 4. Typical load-deflection curve of a coated carbon/carbon in four point flexure at room temperature.

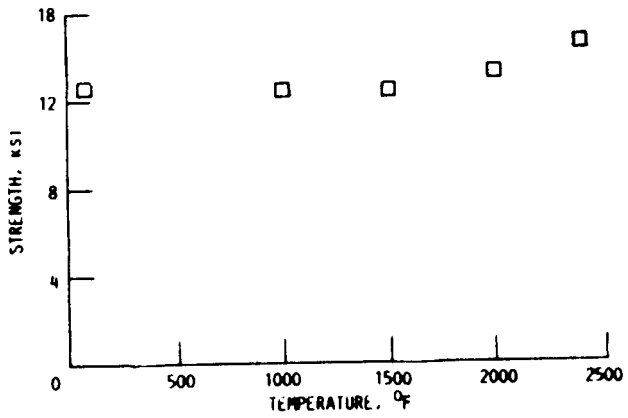


Figure 5. Plot of the flexure strength versus temperature.

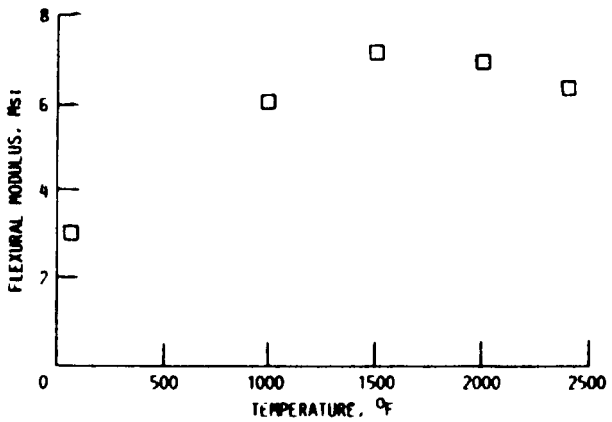


Figure 6. Plot of elastic modulus versus temperature.

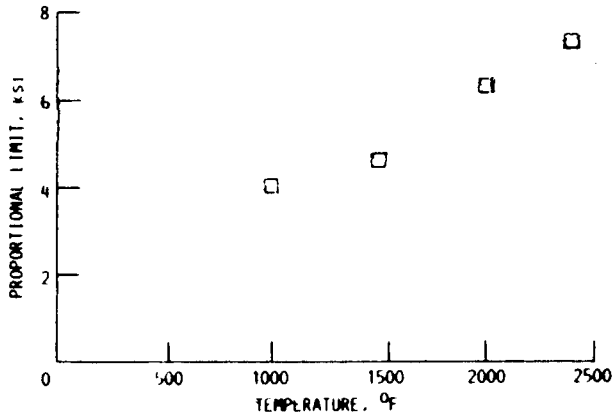


Figure 7. Plot of the proportional limit versus temperature.

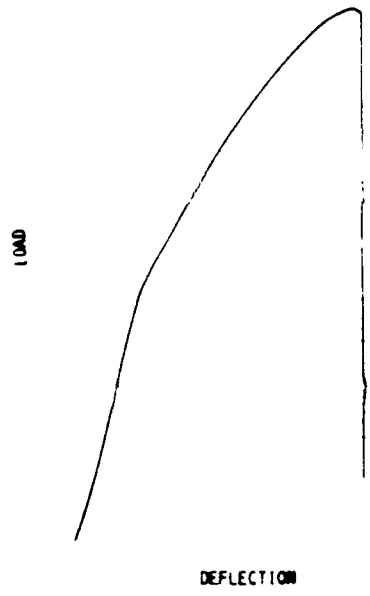


Figure 8. Type I load-deflection curve of a coated carbon/carbon at 2400°F (1316°C) in four point flexure.

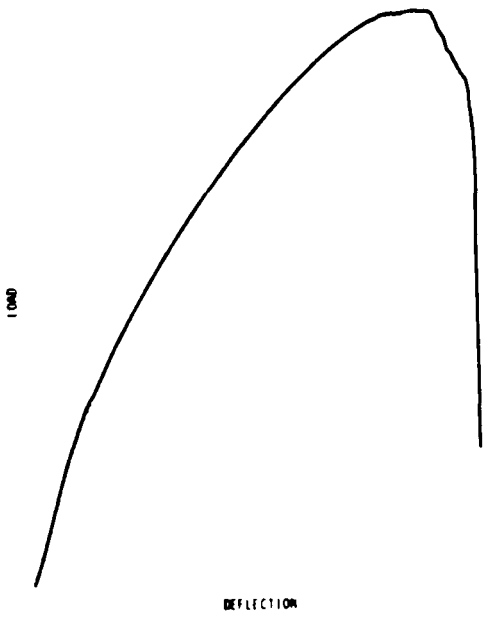


Figure 9. Type II load-deflection curve of a coated carbon/carbon at 1000°F (538°C) in four point flexure.

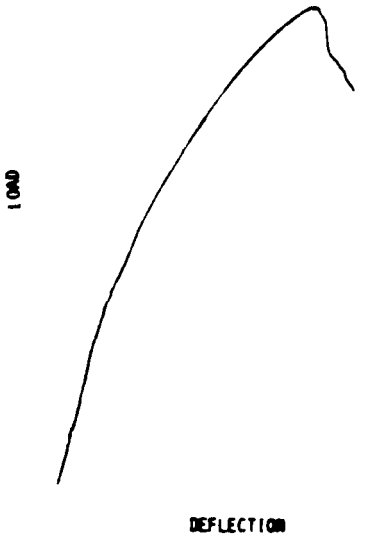


Figure 10. Type III load-deflection curve of a carbon/carbon at 1500°F (816°C) in four point flexure.

ORIGINAL PAGE IS
OF POOR QUALITY

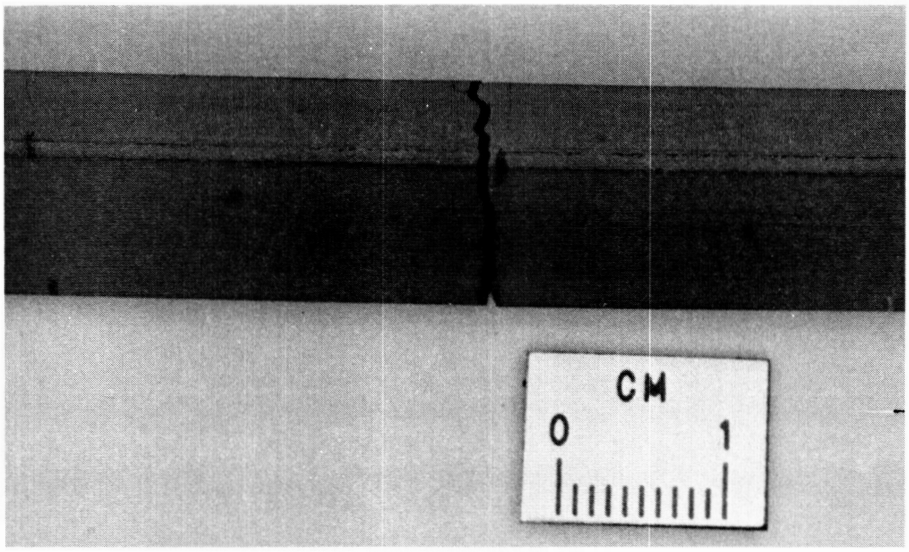


Figure 11. Typical single crack fracture mode in stress rupture, specimen 2-34 at 1000°F (538°C) and 6500 psi (45 MPa).

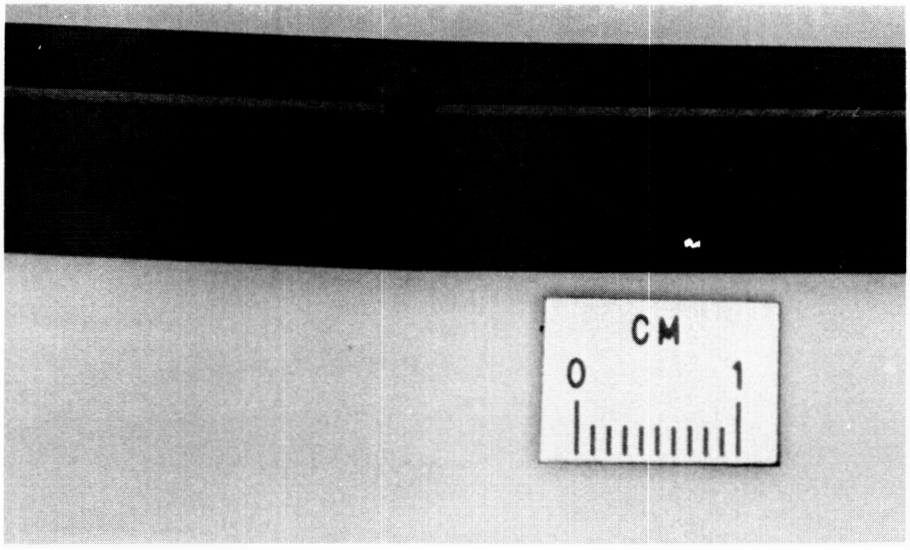


Figure 12. Typical split crack fracture mode in stress rupture specimen 0-13 at 1500°F (816°C) and 6500 psi (45 MPa).

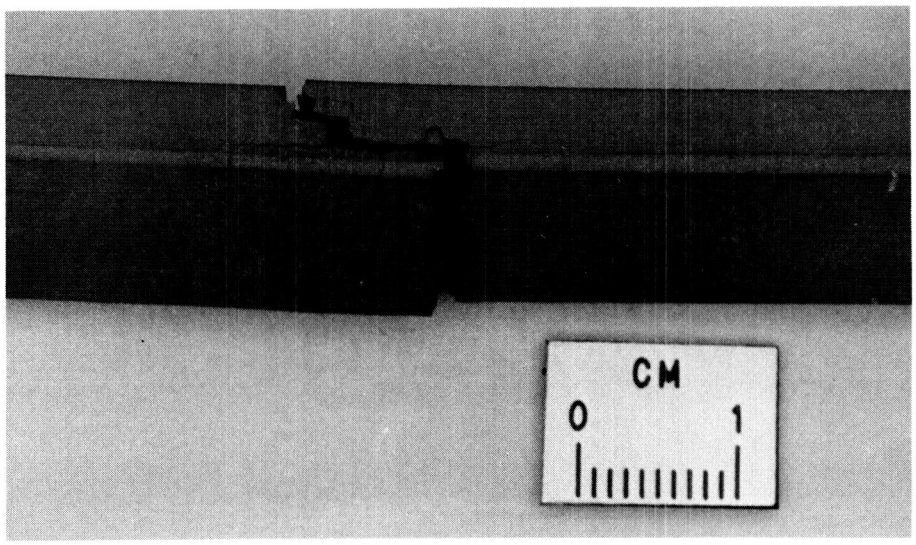


Figure 13. Typical ply shearing fracture mode in stress rupture specimen 2-02 at 1000°F (538°C) and 8000 psi (55 MPa).

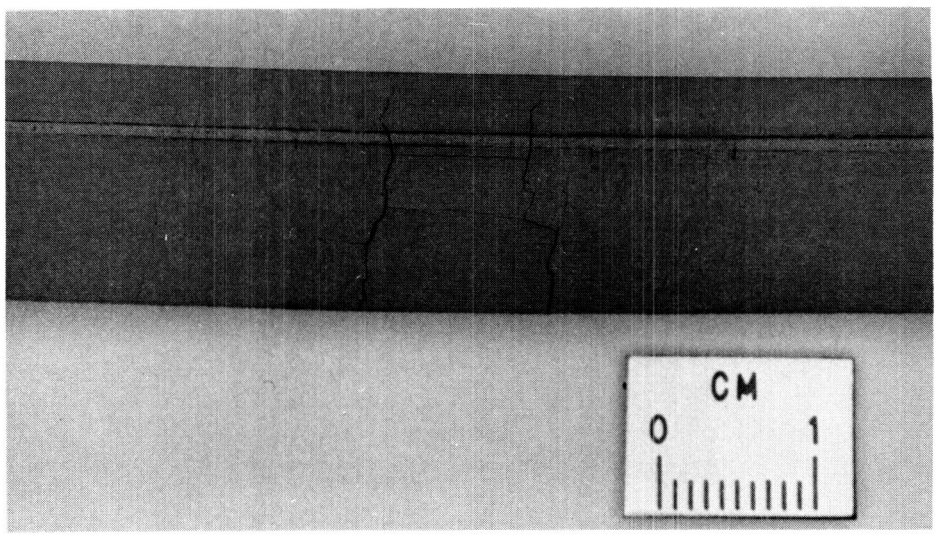


Figure 14. Typical wide fracture mode in stress rupture specimen 2-07 at 1000°F (538°C) and 3600 psi (25 MPa).

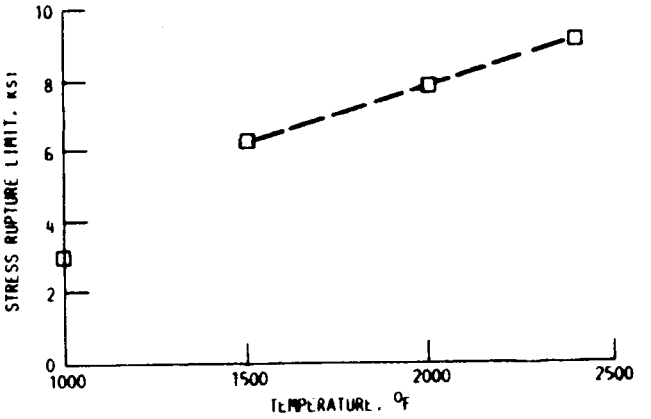


Figure 15. Plot of the stress rupture limit versus temperature.

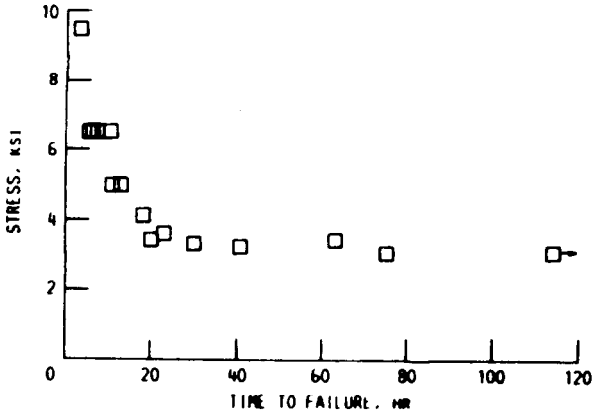


Figure 16. Plot of time to failure versus applied stress at 1000°F.

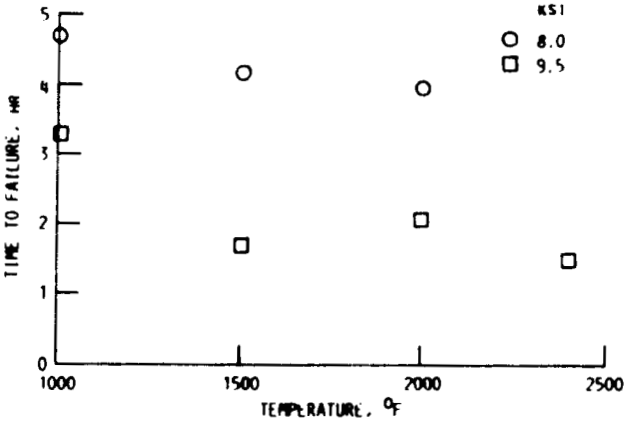


Figure 17. Plot of time to failure versus temperature at stress levels of 8.0 and 9.5 ksi.

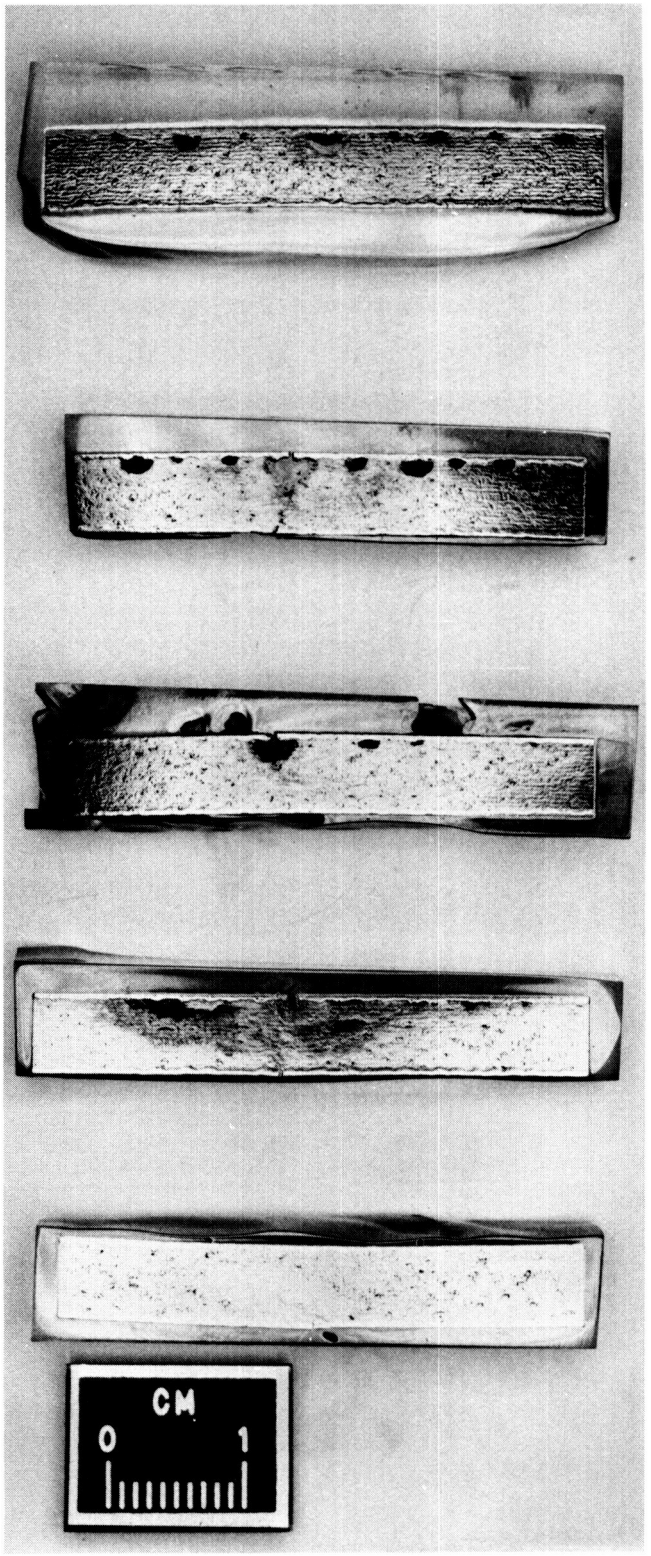


Figure 18. Longitudinal crossection of stress rupture specimens and room temperature flexure specimen.

Appendix A

Procedural Details

## Density Measurement Procedure

The density measurements of the c/c substrate and silicon carbide coating are guided by a wax immersion technique, ASTM C914. The coupons are cut from room temperature flexural specimens with the coupons coming from both sides of the failure zone. The substrate coupons originate from the uncoated specimens and the coated coupons require additional cutting to obtain the coated specimen. The bag and mold sides of the coating are cut away from the substrate with a diamond saw. Some c/c is retained on the "coating coupon" and is removed with an oxidation treatment at 1020°F (550°C) for 20 hours. The ash residue is removed from the coupon. The coating coupons are ultrasonically cleaned in ethanol for 20 hours and then dried at 250°F (120°C) for 12 hours.

The weight of the coupon (CW) is recorded before it is coated with wax. Parafin wax is liquified with a double boiler technique and the coupon is coated by dipping it into the wax. The weight of the wax coated specimen is recorded in air (WCW) and immersed in ethynol (WCI). The temperature of ethanol is recorded to a tenth of a degree and the density is calculated with the following equation:

$$\text{Density} = \frac{CW}{\frac{WCW - WCI}{LD} - \frac{WCW - CW}{WD}} \qquad \text{Eq. A1}$$

CW = Coupon Weight

WCW = Wax Coated Weight

WCI = Wax Coated Immersed Weight

LD = Ethanol

WD = Wax Density

The density of the wax is 0.905 g/cc. The density of the ethanol is determined by interpolation of the temperature, density chart in the CRC handbook*. The data is recorded in Appendix B, Tables B and C.

A density measurement of the pack cementation silicon carbide coating requires the removal of the glass overlay from the coupon. An attempt to measure this density was made. A glass coupon consisting of the coating was placed in a 20% hydroflouric acid solution to dissolve the glass overlay. The coating coupon was completely attacked and only a fine powder remained in the acid after a twelve hour soak.

## Flexural Test Procedures

The details on the determination of the room and elevated temperature flexural properties are presented. Both room and elevated temperature tests were similarly conducted and are described together. The facilities, specimen preparation, calibration, testing procedures and data reduction are summarized for the flexure test at room and

---

* CRC - Handbook of Chemistry and Physics, R. C. Weast, ed., 60th edition, 1979-80, pg. F-6.

elevated temperatures of 1000°, 1500°, 2000°, and 2400°F, (538°, 816°, 1093°, and 1316°C).

The flexural test system is seen in Figure 1A and consisted of a load frame, load cell, water cooled couplings, silicon carbide support and push rods, as silicon carbide resistance heated furnace, and the test fixture. The room temperature tests were conducted in this load train configuration. A 1000 pound capacity load cell was employed to measure the load. The output of the load cell was recorded on a strip chart. This chart also recorded displacement of the crosshead.

The room and elevated temperature test fixtures have the same testing geometry, but were fabricated from different materials. The load fixtures were also different. The room temperature fixture was fabricated from stainless steel as seen in Figure A2 and the elevated temperature fixture from sintered alpha silicon carbide as Figure A3 illustrates. The room temperature loading fixture is loaded at a ball bearing point. The elevated temperature fixture is beveled to insure the point loading of the specimen. The overall width of the room temperature fixture is half of the silicon carbide fixtures used for the high temperature tests.

The testing geometry of this test is four point bending. The support rollers are 1.00 inch in diameter (2.54 cm) and the long support span for flexural failures is 6.12 inches (15.5 cm). The support span in the room temperature test is decreased to 2.00 inches (5.08 cm) with the addition of spacer blocks for the shear tests. The load rollers are 0.44 inches (1.11 cm) in diameter and are in a load span of 1.00 inch (2.54 cm).

The test specimens are coated and uncoated low modulus c/c composites with the approximate dimension of 7.75 long by 0.60 wide by 0.24 inches thick (20 x 1.5 x 0.60 cm). The width and thickness dimensions of each specimen are measured in the high stress zone with vernier calipers to within ±.001 inches (.003 cm). Six coated and eight uncoated specimens are tested at room temperature and five specimens at each of the elevated temperatures. At least one coated specimen from each coating batch are tested at each temperature.

## Calibration

Calibration was required for the load cell, chart speed, cross head deflection, and the compliance of the load train. The 1000 pound capacity load cell was calibrated with weights having calibration traceable to the National Bureau of Standards. The procedure begins after the system warms up for a half an hour. The load train was disassembled and the load cell is placed on the crosshead. The system was electronically zeroed and balanced on the twenty pound scale. The fifty pound scale was selected and fifty pounds of static weights were set on the load cell. This full scale reading was calibrated on the chart recorder. The reading was verified on the one hundred pound scale. The calibration was complete and the load train was reassembled. This calibration procedure was conducted at the beginning of every test day.

The calibration of the chart recorder was a simple procedure. The chart rate was selected, 1.0 inch per minute (2.54 cm/min.). The chart recorder and timer are started simultaneously and stopped after

an interval of two minutes. The expected result was compared with the actual distance travelled. This procedure was conducted once.

The calibration of the crosshead deflection was conducted with a Starret dial indicator for displacement measurements mounted on a magnetic base. The indicator is graduated at 0.0005 inch (.0013 cm) increments. The magnetic base was mounted to the test frame and the spindle of the indicator contacted the crosshead. The dial indicator was zeroed. The crosshead deflection rate was set at 0.05 inches per minute (0.13 cm/min.), and deflected for two minutes. The expected deflection was compared to the measured deflection. This calibration method was conducted once.

The compliance of the load train was measured with the dial indicator that was employed in the previous calibration, and the load which was measured on the strip chart recorder. The silicon carbide test fixture without the load fixture was placed on the support rod. The upper push rod was lowered until it contacted the fixture. The chart recorder was balanced without a load applied. Four pounds of load were applied to the load train by manually lowering the crosshead as indicated on the chart recorder. The dial indicator was zeroed. The crosshead was manually lowered 0.0005 inches and the load and deflection were recorded.

Subsequently, the load train was lowered in 0.0005 inch increments and the loads were recorded. The results from this procedure are as follows:

| Deflection Inches | Load lbs. |
|---|---|
| 0.0000 | 4.0 |
| 0.0005 | 5.3 |
| 0.0010 | 7.4 |
| 0.0015 | 9.2 |
| 0.0020 | 11.6 |
| 0.0025 | 14.9 |
| 0.0030 | 18.9 |
| 0.0035 | 24.8 |
| 0.0040 | 34.1 |
| 0.0045 | 45.1 |
| 0.0050 | 56.8 |
| 0.0055 | 69.5 |

This compliance measurement was conducted once at room temperature and was applied in all modulus calculations. The compliance values at elevated temperatures were assumed to be similar.

## Test Procedures

The test procedure for the conduction of the four point bend flexural tests of coated and uncoated c/c composites involved alignment, heating the furnace, preloading, and calculating the flexural properties. The testing variables of the crosshead speed (0.05 inches per minute) (0.13 cm/min), chart speed (1.0 inches per minute) (2.5 cm/min) and load cell scale (100 pounds) were set at the beginning of the test.

The alignment of the specimen on the support rollers was obtained optically. The mold side of the specimen was in tension. The specimen was centered lengthwise and across the width of the rollers. In the elevated test, the support rollers were bonded to the fixture with an adhesive. The specimens were similarly bonded to the rollers. This maintained the alignment in the transport of the fixture. At elevated temperatures, the adhesive decomposed and the bond was broken. The alignment fixture in Figure A3 was employed to center the load fixture between the support rollers. The load fixture was bonded to the specimen with the adhesive for the elevated temperature test. The test fixture was placed in the load train. Thermocouples were positioned in the maximum stress area. The upper push rod was lowered to within 0.25 inches (0.6 cm) of the load fixture. The furnace was heated to temperature and was soaked at the test temperature for one hour. The pen on the chart recorder was balanced and a preload of four pounds was imposed on the fixture by manually lowering the crosshead. The test was stopped when the load decreased significantly.

The flexure properties of proportional limit, strength, and modulus were calculated after the testing is complete. The values from the chart recorder were used in the calculations. The equations employed in the stress and modulus calculations are based on beam theory. These equations assume that the cross section and elastic constants are homogeneous. Coated and uncoated c/c composites are not homogeneous and invalidate the equations. In lieu of a more rigorous

calculation, the values obtained were used as a first approximation and for comparison within this test sequence.

The test geometries and nomenclature are summarized in Figure 4A. The loads on the strip chart which correspond to the maximum and proportional limit were used in the strength calculations. The slope of the load-deflection curve was measured from the pre-load to the proportional limit and used to calculate the modulus. If no proportional limit was apparent, then the slope from the pre-load to one-half of the maximum load was recorded for the modulus calculation.

The stress was calculated with the following equation:

$$\sigma = \frac{3PKL}{wt^2} \qquad \text{Eq. A2}$$

where $\sigma$ was the strength or proportional limit; P the load; w the width; and t the thickness. The KL value was 2.56 inches (5.5 cm) for the flexure test.

The shear strength, $\tau$, was calculated with the following equation:

$$\tau = \frac{3P}{4wt} \qquad \text{Eq. A3}$$

The modulus, E, was calculated with the following equation:

$$E = \frac{6}{wt^3} \frac{P}{\delta} [KL^3/3 + (KL^2)LS/2 + (KL)LS^2/8] \qquad *\text{Eq. A4}$$

where LS is the load span and P/δ is the load-deflection slope the load span is 1.0 inch (2.54 cm) and the equation reduces to:

$$E = \frac{55.3}{wt^3} \frac{P}{\delta} \qquad \text{Eq. A5}$$

The deflection value, δ, was corrected for the compliance of the load train that was measured.

## Stress Rupture Testing Procedure

The flexural stress rupture properties of coated low modulus carbon/carbon (c/c) composites were examined at the elevated temperature of 1000°, 1500°, 2000°, and 2400°F (538°, 816°, 1093°, and 1316°C). The facilities, calibration, specimen preparation, and procedures of this test are summarized in detail. The test facilities consisted of two compression creep test frames, silicon carbide resistance heated furnaces, silicon carbide test fixtures, extensometry and a data acquisition system (DAS). The compression creep test system were fabricated by Applied Test System and are shown in Figure A5. The test fixture in the load train is pictured in Figure A6 and this fixture was used for the flexure test at elevated temperatures.

* Pears, C.D., H. S. Starret, G. W. Driggers, and D. L. Van Wagoner, "Test Methods for High Temperature Material Characterization", AFML TR 79-4002, 1979. p. 54.

## Extensometry

The extensometry system of the compression creep test system was designed to measure a relative displacement which is described in Appendix C. Figure A7 illustrates the schematic of the extensometry. The probe tips contact the specimen and the relative displacement is transferred through the alumina rods to the extensometer housing. The outer two rods sit on the inner housing and center rod sits on the spring supported core rod. A linear variable differential transformer (LVDT) deflects with the outer rods and measured the displacement. Only the relative displacement of the inner rod to the outer rods affects the output.

## Data Acquisition System

The data acquisition system (DAS) consisted of a IBM PC XT with an interface which was fabricated by Advanced Peripherals Incorporated (API). The API equipment consists of a type "R" thermocouple, voltage input, and a relay modules. Each module contains eight channels for data input or control. These modules are interfaced with the IBM PC XT by an integrated circuit board.

The DAS software was programmed in Basic, and it controlled test parameters and assisted in the calibration of the extensometer. The software controlled the temperature on the extensometer and the flow of air into the test system. The extensometer housing was maintained within 0.5°C of 36°C by a thermocouple and relay channels on the DAS. A heat tape is wrapped around extensometer housing and is connected in series with a relay channel on the DAS. A type "T" (copper

constantan) thermocouple is placed inside the housing and connected to a channel on the thermocouple module. The software read the temperature of the housing every minute and then sent a signal to the relay module to open or close the relay which sent the power to the heat tape.

A similar thermocouple and relay pair were employed to maintain the temperature of the control box to above 34°C. A type "T" thermocouple is placed in the control box and two 75 watt light bulbs are connected in parallel and then in series with a relay of the DAS. The pair of light bulbs is placed at the base of the control box. The temperature of the control box is checked every minute by the DAS.

The DAS controlled the flow of air into the furnace with relay connections to solenoid valves. The flow of compressed air into the furnace was initiated at the start of the test. The air flowed into the furnace at a rate of 10 ml per minute. At failure, the DAS stopped the flow of compressed air and began a purge of nitrogen into the furnace chamber at a rate of 1.0 liter per minute. The nitrogen flow cools the furnace and minimizes the amount of oxidation of the c/c substrate after failure. The purge continued until the temperature was less than 800°F (425°C).

The function of the DAS is the acquisition of data from the stress rupture test. The DAS reads two type "R" (platinum, platinum - 13% rhodium) thermocouples and the output of the LVDT. The thermocouple module converted the millivolt reading to temperature by means of charted values. The strain on the specimens was calculated from the output of the LVDT as explained in the equations of Appendix

C. The time, temperature, and strain were recorded to a data file on the hard disk. The frequency of data storage depended on the test segment. On heat up, soak and cool down, the data was recorded every ten minutes. At the end of the soak period, the LVDT output was zeroed and load applied with procedures described in a later paragraph. Immediately after loading, the data was recorded every minute for the first ten minutes, then every two minutes for the next fifty minutes. At the end of this first hour an algorithm controlled the recording frequency, and is based on the percent increase of strain over the previous recorded value. The frequency is higher when the specimen is straining, as rapidly as once per minute.

## Extensometry Calibration

A DAS software routine allowed the calibration of the extensometer. The procedures involved mechanical manipulations of the extensometer and the calibration micrometer, while the LVDT output voltage is displayed only the screen. The calibration fixture is shown in Figure A8 and the Starret micrometer is graduated in 0.0001 increments. The DAS and electronics of the extensometry required a twenty minute warm up period before operations. The upper push rod was removed from the load train and the calibration fixture was inserted.

Extensometer adjustments and fixture preparation were required at the beginning of calibration. The adjustment screws and micrometer on extensometer housing were lowered to a minimum position. The alignment clip was centered and bonded to the fixture. The test

fixture is then set into the load train with the probe tips of the extensometry extending through the clip. A downward pressure was exerted on the center tip to check for a springy response. This response indicated proper alignment in the extensometer. One quarter inch thick spacer bars were placed on each side of the test fixture. The calibration fixture is set on the spacer bars. The center probe tip contacted the center of the calibration micrometer. The micrometer was positioned where the spindle face was at the same level as the calibration fixture (0.9125 inches).

The next routine determined the level of the adjustment screws for all the stress rupture testing. At this level, the probes will not droop during a test and yield erroneous data. The micrometer in the extensometer housing is raised 0.25 inches (0.6 cm), and the adjustments screws were evenly increased until the outer probes contact the calibration fixture. A downward force was exerted on the micrometer in the extensometry housing and then released. The position of the outer probe was examined. If the probes did not contact the calibration fixture, then the adjustment screws were raised and the response to the downward pressure on the micrometer was rechecked. This iteration continued until a consistent response of probe tips contacting the calibration fixture was obtained. This level was marked on the adjustment screws at the entrance to the housing with an indelible marker.

The mechanical calibration of the LVDT began with the selection of "Display LVDT Voltage" routine from the DAS Main Menu. An electronic zero was obtained before the mechanical calibration. The

toggle switch on the LVDT control panel was set to calibrate and the zero knob is on the control panel was rotated until a zero output was displayed. The toggle switch was returned to the operate position. The micrometer in the extensometer housing was rotated until the output voltage reads zero volts. The LVDT was then calibrated at one-half full scale deflection. The calibration micrometer was deflected one-half full scale (0.015 inches) (.038 cm) and the output voltage was 5.00 volts for perfect calibration. This voltage was obtained by rotating the range knob on the LVDT control panel. The calibration micrometer was returned to the zero position by exceeding the zero value and then approaching it with a downward direction of the micrometer. A zero voltage was not displayed at the zero level and was obtained by rotating the micrometer in the housing until zero volts is displayed. The calibration started again with a half scale deflection and an iteration of deflections and range knob adjustments were required to calibrate.

## Stress Rupture Testing

The stress rupture test procedures involved the alignment and loading of the specimen prior to the operations of the test. The alignment of the specimen, load train and extensometry are required before heating the furnace. At the beginning of the aligning procedures, the data acquisition system (DAS) and extensometry power was turned on and allowed to warm up.

The alignment of the specimen in the test fixture was accomplished with a ruler and an epoxy adhesive. This bonding was

conducted to maintain alignment during handling. The epoxy decomposed and the bond was destroyed at elevated temperatures. The support rollers were bonded with epoxy to the fixture. The mold side of the specimen was placed downward on the tension side. The length-wise alignment of the specimen on the support rollers was obtained optically by approximating an equal overhanging distance of the specimen over the support roller. Alignment of the specimen across the width involved maneuvering the specimen until the distance between the specimen edge and the edge of support roller was equivalent on either side of the specimen. This distance was measured with a ruler. The specimen was then bonded to the rollers.

Adjustments to the extensometry were necessary to minimize the possibility of fracturing the probes while inserting the fixture into the load train. The inner housing of the extensometry was lowered to a minimum position by decreasing the adjustment screws and micrometer head at the base of the extensometry housing. Misalignment of the center tip in the extensometry commonly occurred and the proper alignment was needed before inserting the test fixture. A downward force was applied to the center tip and the resistance to the force was either springy or rigid. A rigid response indicated non-alignment. Alignment was obtained by raising the micrometer head and maneuvering the center rod until the response was springy.

Mechanical adjustments to the test frame and extensometry were required to position the test fixture in the load train. The upper push rod is raised and the test fixture was placed in the load train with the extensometry probes extending through the fixture. The

alignment of the center tip was rechecked with the previously described procedure. The inner housing is raised with the adjustment screws until the center probe contacted the specimen. The "Display LVDT Voltage" routine was selected from the DAS menu. The output voltage was adjusted to a value between negative four and five volts by increasing the micrometer head. The DAS was then returned to the DAS main menu.

The load fixture was aligned on the specimen after the thermocouples were placed in the maximum stress area. The load fixture was placed on the specimen and an alignment device, Figure A9, centered the load fixture between the support rollers. The load fixture was aligned across the width by the grooves machined in the alignment pins. The upper push rod was lowered to one quarter inch above the load fixture. The furnace heat up was initiated by selecting the "Initiate Test" routine from the DAS menu. The test variables were input as the DAS prompts and heat up begins.

Once at test temperature, some adjustments to the test system were performed. The upper push rod was lowered until it contacted the load fixture. The "Display LVDT Voltage" routine was selected on the DAS menu. The adjustment screws on extensometry were raised one quarter of an inch and the micrometer head is raised until the output voltage was between negative three and four volts. The DAS was then returned to the main menu. The furnace equilibrated for one hour before loading the specimen.

Preparation of the test system for the application of stress to the specimen began with calculating the weight required to load a

specimen to a desired stress level. This weight less the weight of the load train was added to the weight platen. The "Display LVDT Voltage" routine was chosen from the DAS menu. The extensometry adjustment screws were raised to the level marked on the screws during the calibration procedures. The micrometer head was adjusted until the output was within one-tenth of a volt from zero.

The "Zeroing" routine was selected from the "Display Voltage" routine. The DAS read and recorded the initial voltage as the zero voltage. Subsequent LVDT readings were reduced by the zero voltage prior to calculating the strain. The load was then applied to the specimen by lowering the bolt that supports the weight platen at ten seconds before the next reading. The remainder of the test was controlled by the DAS as previously described.

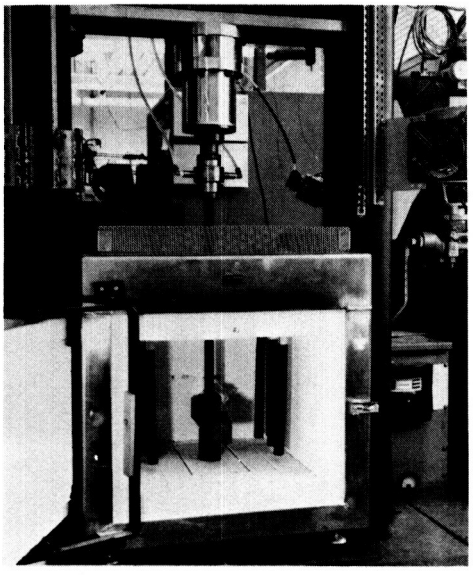

Figure A1. Flexure test load frame.

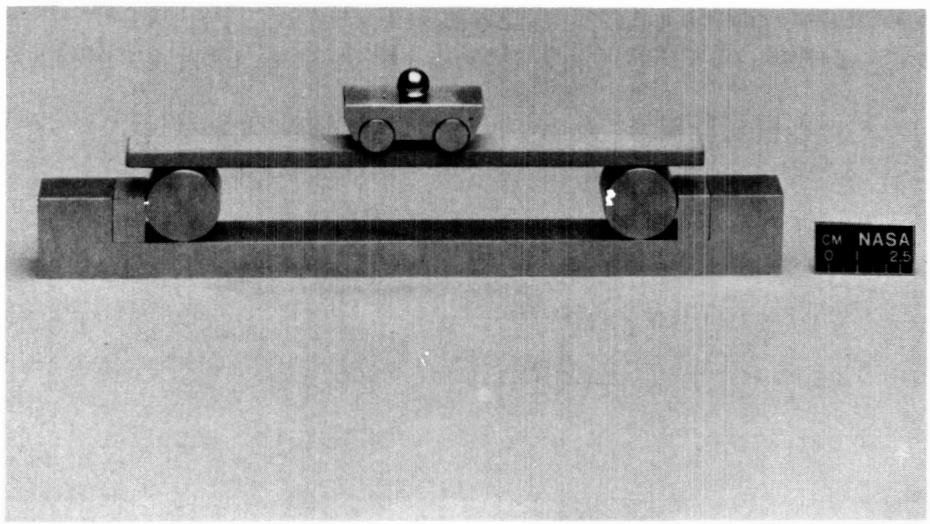


Figure A2. Room temperature flexure text fixture.

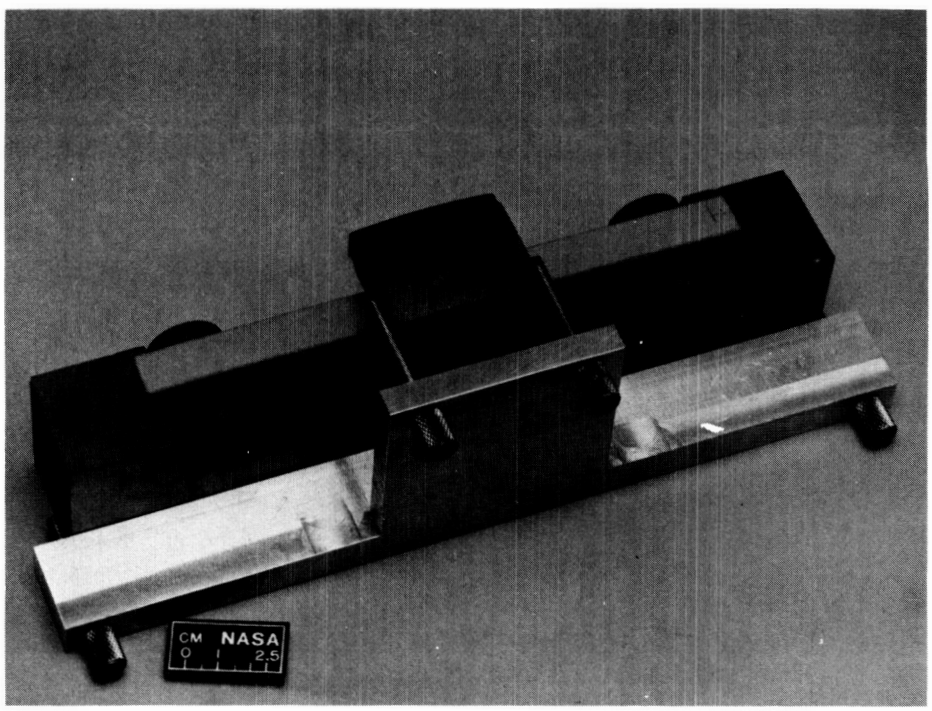


Figure A3. Elevated temperature flexure test fixture with centering fixture.

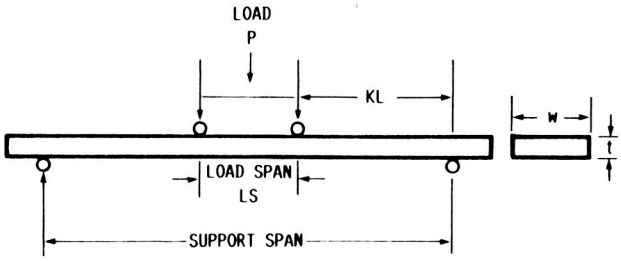


Figure A4. Flexure geometry nomenclature.

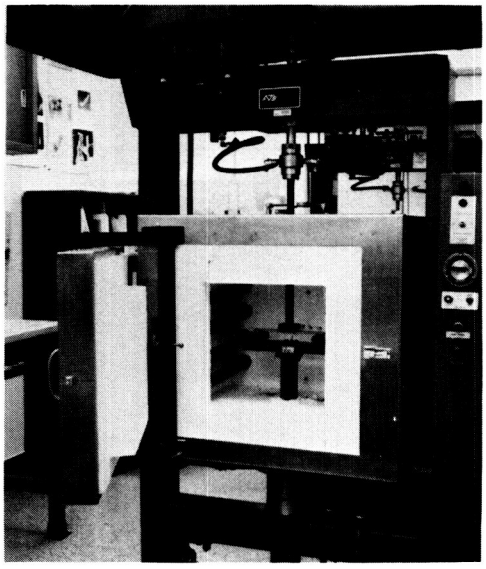

Figure A5. Stress rupture test frame.

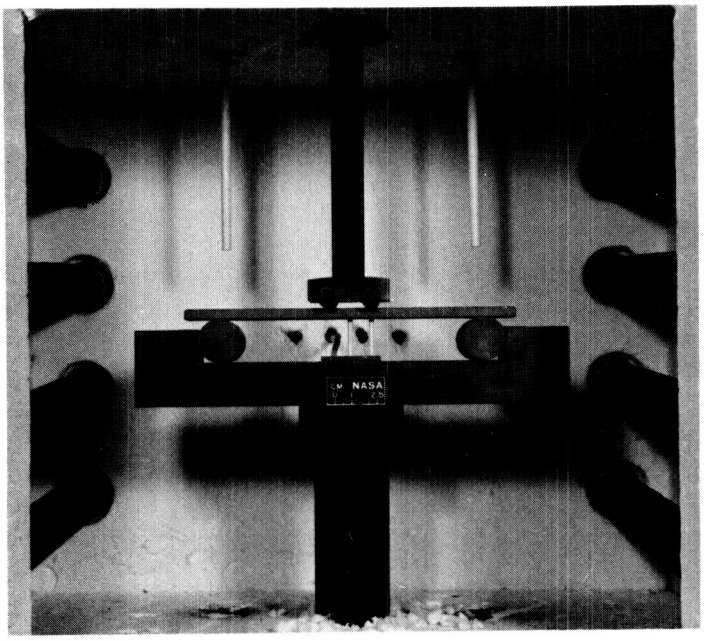

Figure A6. Test fixture in load train.

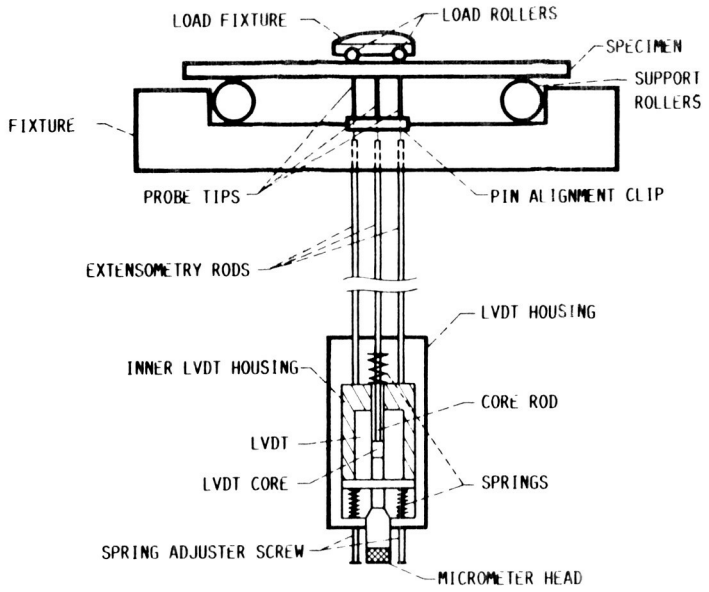


Figure A7. Extensometry for stress rupture test.

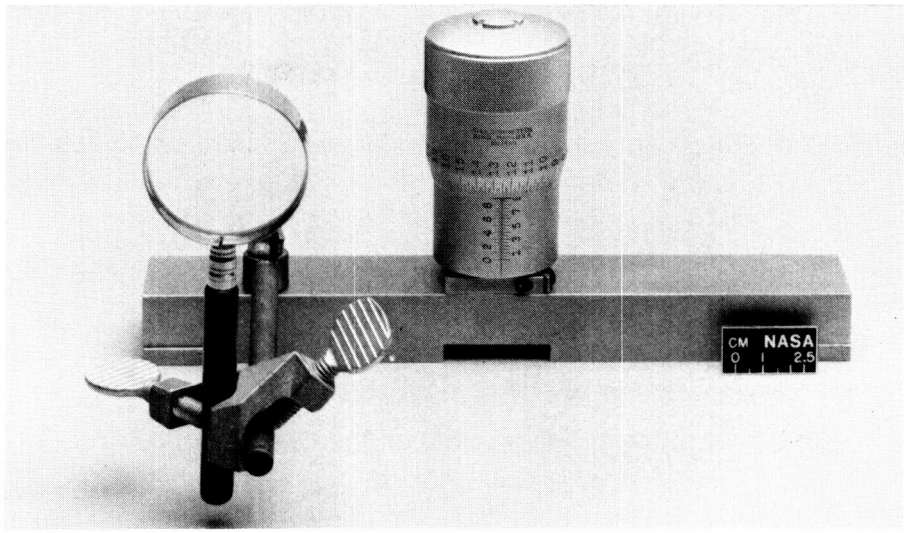


Figure A8. Calibration fixture.

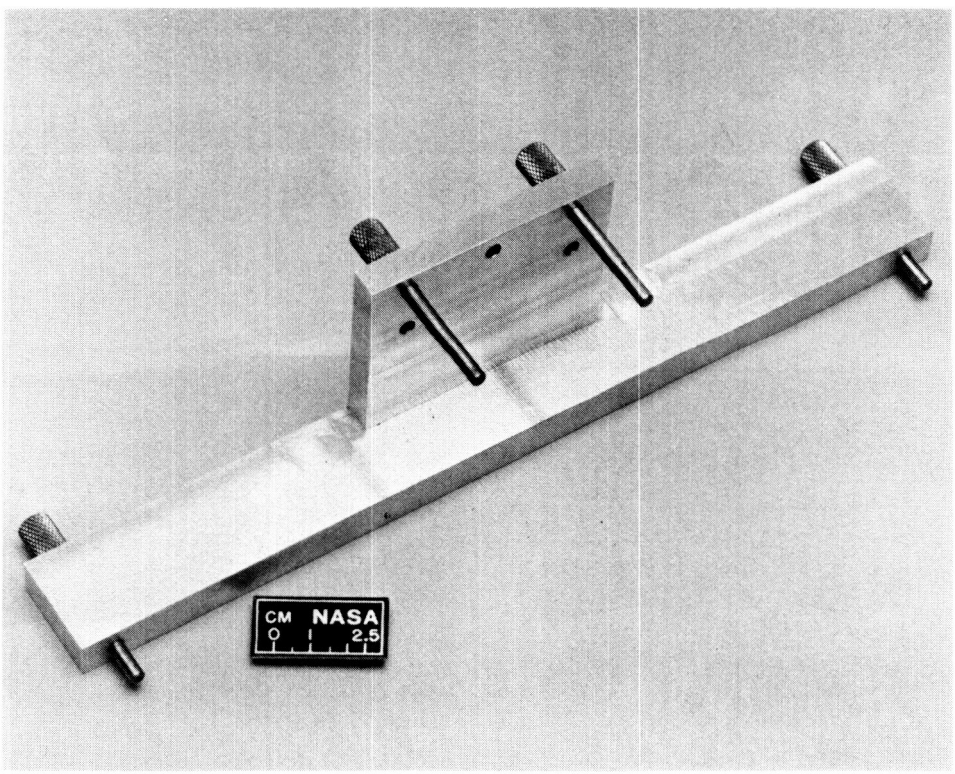


Figure A9. Centering fixture.

Appendix B

TABLES

TABLE A

Designation of Specimen Number, Panel Number, Coating Batch Number

Carbon/Carbon

| Coating Batch 0 | Panel Number | Specimen Numbers |
|---|---|---|
| | 2 | 0-01 to 0-18 |
| | 3 | 0-19 to 0-38 |
| | 5 | 0-39 to 0-49 |
| | 8 | 0-50 |
| Coating Batch 1 | 6 | 1-02 to 1-07 |
| | 6 | 1-09 to 1-14 |
| | 6 | 1-16 to 1-18 |
| | 7 | 1-19 to 1-21 |
| | 7 | 1-23 to 1-28 |
| | 7 | 1-30 to 1-35 |
| | 8 | 1-37 to 1-43 |
| Coating Batch 2 | 8 | 2-01 to 2-08 |
| | 9 | 2-50 |
| | 9 | 2-09 to 2-26 |
| | 10 | 2-27 to 2-45 |
| | 11 | 2-46 to 2-49 |

TABLE B

Density of Low Modulus Carbon/Carbon Substrate

| Specimen | Density Values g/cc A | B | C | D | Average |
|---|---|---|---|---|---|
| 19 | 1.382 | 1.377 | 1.374 | 1.374 | 1.377 |
| 89 | 1.379 | 1.379 | 1.380 | 1.382 | 1.380 |
| 159 | 1.381 | 1.378 | 1.377 | 1.376 | 1.378 |
| Overall Average | | | | | 1.378 g/cc |

TABLE C

Density of Silicon Carbide Coating

| Batch Number | Specimen Side | Density g/cc | g/cc | Average Density |
|---|---|---|---|---|
| 0 | Bag | 2.61 | 2.61 | 2.61 |
| 0 | Mold | 2.61 | - | 2.61 |
| 1 | Bag | 2.57 | 2.70 | 2.64 |
| 1 | Mold | 2.58 | 2.60 | 2.59 |
| 2 | Bag | 2.63 | 2.71 | 2.67 |
| 2 | Mold | 2.61 | 2.75 | 2.69 |
| Overall Average | | | | 2.63 g/cc |

TABLE D

Summary of the Coating Thickness Measurements

| Number of Data Points | Side Type | Average Coating Thickness (ins.) | Standard Deviation | Maximum Value (ins.) | Minimum Value (ins.) | Glass Layer Average Thickness (ins.) |
|---|---|---|---|---|---|---|
| Batch '0 Warp Yarns Parallel to Coating | | | | | | |
| 12 | Edge | 0.024 | 0.004 | 0.031 | 0.017 | 0.002 |
| 24 | Bag | 0.014 | 0.004 | 0.022 | 0.008 | 0.001 |
| 22 | Mold | 0.013 | 0.002 | 0.017 | 0.009 | 0.002 |
| Batch '0 Fill Yarns Parallel to Coating | | | | | | |
| 12 | Edge | 0.032 | 0.005 | 0.042 | 0.023 | 0.002 |
| 12 | Bag | 0.011 | 0.001 | 0.012 | 0.010 | 0.001 |
| 12 | Mold | 0.012 | 0.003 | 0.018 | 0.008 | 0.001 |
| Batch '1 Warp Yarns Parallel to Coating | | | | | | |
| 8 | Edge | 0.023 | 0.004 | 0.029 | 0.017 | 0.006 |
| 24 | Bag | 0.017 | 0.003 | 0.024 | 0.011 | 0.002 |
| 24 | Mold | 0.014 | 0.004 | 0.020 | 0.005 | 0.002 |
| Batch '1 Fill Yarns Parallel to Coating | | | | | | |
| 10 | Edge | 0.029 | 0.004 | 0.037 | 0.021 | 0.008 |
| 12 | Bag | 0.016 | 0.003 | 0.023 | 0.008 | 0.004 |
| 12 | Mold | 0.016 | 0.003 | 0.020 | 0.013 | 0.002 |
| Batch '2 Warp Yarns Parallel to Coating | | | | | | |
| 12 | Edge | 0.023 | 0.003 | 0.028 | 0.017 | 0.001 |
| 24 | Bag | 0.012 | 0.002 | 0.019 | 0.009 | 0.001 |
| 24 | Mold | 0.012 | 0.002 | 0.019 | 0.008 | 0.002 |
| Batch '2 Fill Yarns Parallel to Coating | | | | | | |
| 9 | Edge | 0.028 | 0.003 | 0.032 | 0.003 | 0.002 |
| 12 | Bag | 0.011 | 0.002 | 0.014 | 0.007 | 0.002 |
| 12 | Mold | 0.012 | 0.003 | 0.016 | 0.009 | 0.001 |

TABLE E

Chemical Analysis of SiC Coating on RCC-3 Substrate

| Batch | Side | Aluminum | Boron | Calcium | Iron | Sodium | Silicon |
|---|---|---|---|---|---|---|---|
| 0 | Mold | 0.2 | 0.09 | 1.3 | 0.02 | 0.4 | 32.8 |
| 0 | Bag | 0.2 | 0.09 | 0.04 | 0.02 | 0.3 | 33.0 |
| 1 | Mold | 0.1 | 0.1 | 0.04 | 0.02 | 0.3 | 35.3 |
| 1 | Bag | 0.1 | 0.1 | 0.03 | 0.02 | 0.4 | 33.6 |
| 2 | Mold | 0.1 | 0.07 | 0.03 | 0.01 | 0.2 | 34.2 |
| 2 | Bag | 0.1 | 0.1 | 0.02 | 0.01 | 0.3 | 35.4 |

TABLE F

Chemical Analysis of C-C Substrate Ash After Coating

| Batch | Side | Aluminum | Boron | Calcium | Iron | Sodium | Silicon |
|---|---|---|---|---|---|---|---|
| 0 | Mold | 0.9 | 0.7 | 0.2 | 0.2 | 2.0 | 71.7 |
| 0 | Bag | 0.4 | 0.7 | 0.1 | 1.7 | 1.4 | 38.4 |
| 1 | Mold | 0.6 | 0.4 | 0.2 | 0.2 | 1.0 | 30.5 |
| 1 | Bag | 0.5 | 0.3 | 0.1 | 0.1 | 0.6 | 17.5 |
| 2 | Mold | 0.2 | 0.4 | 0.1 | 0.1 | 1.1 | 25.8 |
| 2 | Bag | 0.3 | 0.9 | 0.1 | 0.2 | 1.8 | 34.3 |

TABLE G

X-Ray Diffraction Analysis of SiC Coating

| | Batch "0" | | Batch "1" | | Batch "2" | |
|---|---|---|---|---|---|---|
| Peaks | Mold | Bag | Mold | Bag | Mold | Bag |
| 1 | 2.53 | 2.52 | 2.51 | 2.54 | 2.54 | 2.54 |
| 2 | 1.54 | 1.54 | 1.54 | 1.55 | 1.54 | 1.55 |
| 3 | 1.32 | 1.32 | 1.31 | 1.32 | 1.32 | 1.32 |
| 4 | 2.64 | 2.63 | 2.34 | 2.66 | 2.38 | 2.65 |
| 5 | 2.37 | 2.36 | 2.62 | 2.38 | 2.65 | 2.38 |
| 6 | 2.59 | 2.58 | 2.57 | 2.60 | 2.60 | 1.43 |
| 7 | 2.67 | 1.25 | 2.17 | 1.43 | 1.42 | 2.61 |
| 8 | 1.42 | 1.42 | 1.42 | 2.20 | 2.20 | 2.69 |
| Major Phase | βSiC | βSiC | βSiC | βSiC | βSiC | βSiC |
| Minor Phase | αSiC | αSiC | αSiC | αSiC | αSiC | αSiC |

TABLE H

Room Temperature Flexural Strengths of Uncoated Specimens

| Specimen Number | Panel Number | Flexural Strength | | Flexural Modulus | | Failure Type |
|---|---|---|---|---|---|---|
| | | ksi | MPa | Msi | GPa | |
| 19 | 2 | 13.7 | 94 | 2.3 | 16 | Partial |
| 46 | 3 | 13.6 | 94 | 2.7 | 19 | Complete |
| 69 | 5 | 13.7 | 94 | 2.4 | 17 | Partial |
| 89 | 6 | 13.6 | 94 | 2.3 | 16 | Complete |
| 135 | 8 | 13.1 | 90 | 2.2 | 15 | Partial |
| 159 | 9 | 14.1 | 97 | 2.4 | 17 | Partial |
| 184 | 10 | 14.0 | 97 | 2.2 | 15 | Partial |
| 196 | 11 | 12.8 | 88 | 2.0 | 14 | Partial |
| Average | | 13.6 | 94 | 2.3 | 15 | |
| Standard Deviation | | 0.4 | 3 | 0.2 | 1 | |

TABLE I

Room Temperature Flexural Strengths of Coated Specimens

| Specimen Number | Panel Number | Flexural Strength | | Flexural Modulus | | Failure Type |
|---|---|---|---|---|---|---|
| | | ksi | MPa | Msi | GPa | |
| 0-17 | 2 | 12.7 | 88 | 3.1 | 21 | Partial |
| 0-18 | 2 | 13.0 | 90 | 2.7 | 19 | Partial |
| 1-17 | 6 | 12.9 | 89 | 3.0 | 21 | Partial |
| 1-18 | 6 | 12.3 | 85 | 2.9 | 20 | Complete |
| 2-26 | 9 | 12.1 | 83 | 3.0 | 21 | Partial |
| 2-27 | 9 | 13.5 | 93 | 3.4 | 23 | Partial |
| Average | | 12.8 | 88 | 3.0 | 21 | |
| Standard Deviation | | | 0.5 | 3 | 0.2 | 1 |

TABLE J

Room Temperature Shear Strengths of Uncoated Specimens

| Specimen Number | Panel Number | Shear Stress at Failure | | Flexural Stress at Failure | |
|---|---|---|---|---|---|
| | | ksi | MPa | ksi | MPa |
| 45 | 3 | 2.6 | 18 | 12.9 | 89 |
| 112 | 7 | 2.4 | 17 | 12.0 | 83 |
| 183 | 10 | 2.5 | 17 | 12.8 | 88 |
| Average | | 2.5 | 17 | 12.6 | 87 |

TABLE K

Room Temperature Shear Strengths of Coated Specimens

| Specimen Number | Panel Number | Shear Stress at Failure | | Flexural Stress at Failure | |
|---|---|---|---|---|---|
| | | ksi | MPa | ksi | MPa |
| 0-37 | 3 | 2.9 | 20 | 14.6 | 101 |
| 1-35 | 7 | 2.4 | 17 | 12.4 | 86 |
| 2-45 | 10 | 2.7 | 18 | 13.9 | 96 |
| Average | | 2.7 | 18 | 13.6 | 94 |

TABLE L

1000°F Flexural Strengths

| Specimen | Panel | Flexure Strength ksi | MPa | Proportional Limit ksi | MPa | Flexure Modulus Msi | GPa | Deflection in. | cm. | Failure Type | Defl. Curve Type |
|---|---|---|---|---|---|---|---|---|---|---|---|
| 0-04 | 2 | 12.7 | 88 | 4.1 | 28 | 5.5 | 38 | 0.14 | 0.35 | Partial | I |
| 0-32 | 3 | 12.2 | 84 | 3.9 | 27 | 6.4 | 44 | 0.13 | 0.33 | Partial | I |
| 1-12 | 6 | 12.4 | 86 | 4.7 | 32 | 5.4 | 37 | 0.15 | 0.37 | Complete | I |
| 2-04 | 8 | 12.2 | 84 | 3.8 | 26 | 5.8 | 40 | 0.13 | 0.34 | Complete | I |
| 2-32 | 10 | 12.3 | 85 | 3.6 | 25 | 6.9 | 48 | 0.16 | 0.40 | Partial | II |
| Average | | 12.4 | 85 | 4.0 | 28 | 6.0 | 41 | 0.14 | 0.36 | | |
| Standard Deviation | | 0.2 | 1 | 0.4 | 3 | 0.6 | 4 | 0.01 | 0.03 | | |

TABLE M

1500°F Flexural Strengths

| Specimen | Panel | Flexure Strength ksi | MPa | Proportional Limit ksi | MPa | Flexure Modulus Msi | GPa | Deflection in. | cm. | Failure Type | Defl. Curve Type |
|---|---|---|---|---|---|---|---|---|---|---|---|
| 0-12 | 2 | 12.0 | 83 | 4.8 | 33 | 7.0 | 49 | 0.13 | 0.34 | Partial | III |
| 0-42 | 5 | 12.8 | 88 | 4.4 | 30 | 6.7 | 46 | 0.14 | 0.35 | Partial | III |
| 1-28 | 7 | 12.6 | 87 | 4.5 | 31 | 7.1 | 49 | 0.12 | 0.32 | Partial | III |
| 2-40 | 10 | 12.6 | 87 | 4.6 | 32 | 6.5 | 45 | 0.13 | 0.34 | Partial | III |
| 2-50 | 9 | 12.1 | 83 | 4.7 | 32 | 7.7 | 53 | 0.12 | 0.30 | Partial | III |
| Average | | 12.4 | 86 | 4.6 | 32 | 7.0 | 48 | 0.13 | 0.33 | | |
| Standard Deviation | | 0.3 | 2 | 0.2 | 1 | 0.4 | 3 | 0.01 | 0.02 | | |

TABLE N

2000°F Flexural Strengths

| Specimen | Panel | Flexure Strength ksi | MPa | Proportional Limit ksi | MPa | Flexure Modulus Msi | GPa | Deflection in. | cm. | Failure Type | Defl. Curve Type |
|---|---|---|---|---|---|---|---|---|---|---|---|
| 0-19 | 3 | 12.8 | 88 | 6.2 | 42 | 7.3 | 50 | 0.11 | 0.29 | Partial | I |
| 0-49 | 5 | 13.8 | 95 | 5.9 | 41 | 6.9 | 48 | 0.14 | 0.35 | Partial | I |
| 1-19 | 7 | 13.8 | 95 | 6.7 | 46 | 6.9 | 48 | 0.13 | 0.33 | Partial | I |
| 1-31 | 7 | 12.8 | 88 | 6.4 | 44 | 6.5 | 45 | 0.13 | 0.32 | Partial | I |
| 2.17 | 9 | 13.5 | 93 | 6.3 | 43 | 6.6 | 46 | 0.15 | 0.38 | Partial | I |
| Average | | 13.3 | 92 | 6.3 | 44 | 6.8 | 47 | 0.13 | 0.33 | | |
| Standard Deviation | | 0.5 | 3 | 0.3 | 2 | 0.3 | 2 | 0.01 | 0.03 | | |

TABLE O

2400°F Flexural Strengths

| Specimen | Panel | Flexure Strength ksi | MPa | Proportional Limit ksi | MPa | Flexure Modulus Msi | GPa | Deflection in. | cm. | Failure Type | Defl. Curve Type |
|---|---|---|---|---|---|---|---|---|---|---|---|
| 0-27 | 3 | 14.2 | 98 | 7.0 | 48 | 6.2 | 43 | 0.14 | 0.35 | Partial | I |
| 1-03 | 6 | 14.7 | 101 | 7.6 | 53 | 7.2 | 50 | 0.14 | 0.35 | Partial | I |
| 1-41 | 8 | 14.2 | 98 | 7.1 | 49 | 6.0 | 41 | 0.14 | 0.36 | Partial | I |
| 2-25 | 9 | 14.6 | 101 | 7.3 | 50 | 6.4 | 44 | 0.16 | 0.40 | Partial | I |
| 2-49 | 11 | 15.2 | 105 | 7.5 | 52 | 6.2 | 43 | 0.16 | 0.40 | Partial | I |
| Average | | 14.6 | 101 | 7.3 | 51 | 6.4 | 44 | 0.15 | 0.37 | | |
| Standard Deviation | | 0.4 | 3 | 0.3 | 2 | 0.4 | 3 | 0.01 | 0.02 | | |

TABLE P

1000°F Stress Rupture Summary

| Number | Panel | Stress MPa | ksi | Time of Test hours | Failure Type | Number Optical Cracks | Initial Strain Rate |
|---|---|---|---|---|---|---|---|
| 0-31 | 3 | 21 | 3.0 | 130 | * | 0 | -- |
| 2-30 | 10 | 21 | 3.0 | 130 | * | 0 | -- |
| 2-33 | 10 | 21 | 3.1 | 114 | * | - | -- |
| 2-31 | 10 | 21 | 3.1 | 75 | Single | 2 | -- |
| 1-06 | 6 | 22 | 3.2 | 460 | * | 0 | -- |
| 0-36 | 3 | 22 | 3.2 | 41 | Split | 2 | -- |
| 1-13 | 6 | 23 | 3.3 | 30 | Single | 3 | 0.15 |
| 0-05 | 2 | 23 | 3.4 | 63 | Single | 1 | 1.02 |
| 0-30 | 3 | 23 | 3.4 | 20 | Split | 3 | 0.18 |
| 2-07 | 8 | 25 | 3.6 | 23 | Wide | 5 | 0.10 |
| 1-11 | 6 | 28 | 4.1 | 18 | Split | 4 | -- |
| 1-07 | 6 | 34 | 5.0 | 13 | Shear | 11 | 0.14 |
| 2-01 | 8 | 34 | 5.0 | 10.9 | Shear | 9 | 0.40 |
| 1-05 | 6 | 45 | 6.5 | 10.6 | Shear | 7 | 0.60 |
| 2-05 | 8 | 45 | 6.5 | 7.1 | Shear | 8 | 0.62 |
| 0-02 | 2 | 45 | 6.5 | 6.4 | Shear | 7 | 0.70 |
| 2-34 | 10 | 45 | 6.5 | 5.1 | Single | 4 | 0.57 |
| 1-21 | 7 | 55 | 8.0 | 5 | Shear | 5 | 0.62 |
| 0-35 | 3 | 55 | 8.0 | 4.7 | Shear | 12 | 0.56 |
| 2-02 | 6 | 55 | 8.0 | 4.3 | Shear | 6 | 0.63 |
| 1-09 | 6 | 65 | 9.5 | 3.2 | Single | 5 | 0.51 |
| 0-33 | 3 | 65 | 9.5 | 3.1 | Shear | 8 | 0.81 |
| 2-28 | 10 | 65 | 9.5 | 2.8 | Wide | 9 | 0.66 |

* indicates no failure

TABLE Q

1500°F Stress Rupture Summary

| Number | Panel | Stress MPa | Stress ksi | Time of Test hours | Failure Type | Number Optical Cracks | Initial Strain Rate |
|---|---|---|---|---|---|---|---|
| 2-11 | 9 | 32 | 4.6 | 228 | * | - | -- |
| 1-27 | 7 | 43 | 6.3 | 122 | * | 1 | 0.15 |
| 1-23 | 7 | 44 | 6.4 | 27 | Single | - | 0.23 |
| 0-09 | 2 | 44 | 6.4 | 100 | * | 2 | 0.16 |
| 2-12 | 9 | 44 | 6.4 | 165 | * | 1 | 0.55 |
| 1-30 | 7 | 45 | 6.5 | 8 | Split | 5 | 0.72 |
| 0-13 | 2 | 45 | 6.5 | 58 | Split | 6 | 0.39 |
| 2-41 | 10 | 45 | 6.5 | 160 | * | 1 | 0.46 |
| 0-41 | 5 | 45 | 6.6 | 10 | Single | 4 | 0.44 |
| 2-39 | 10 | 47 | 6.8 | 12 | Split | 1 | 0.23 |
| 0-11 | 2 | 48 | 7.0 | 6.9 | Split | 7 | 0.19 |
| 0-40 | 5 | 55 | 8.0 | 3.9 | Split | 10 | 0.44 |
| 2-37 | 10 | 55 | 8.0 | 5 | Single | 6 | 0.45 |
| 0-10 | 2 | 65 | 9.5 | 1.4 | Split | 14 | 0.78 |
| 1-25 | 7 | 65 | 9.5 | 1.6 | Single | - | 0.55 |
| 2-38 | 10 | 65 | 9.5 | 2.2 | Single | 16 | 0.44 |

* indicates no failure

TABLE R

2000°F Stress Rupture Summary

| Number | Panel | Stress MPa | Stress ksi | Time of Test hours | Failure Type | Number Optical Cracks | Initial Strain Rate |
|---|---|---|---|---|---|---|---|
| 0-20 | 3 | 46 | 6.7 | 235 | * | - | 0.74 |
| 2-20 | 9 | 53 | 7.7 | 137 | * | 4 | 0.18 |
| 0-22 | 3 | 54 | 7.9 | 100 | * | - | -- |
| 1-16 | 6 | 54 | 7.9 | 126 | * | 6 | -- |
| 2-16 | 9 | 55 | 8 | 3.2 | Single | 7 | 0.98 |
| 1-32 | 7 | 55 | 8 | 3.7 | Single | - | -- |
| 0-47 | 5 | 55 | 8 | 5 | Single | 5 | 0.43 |
| 2-42 | 10 | 55 | 8 | 300 | * | 14 | 0.74 |
| 0-48 | 5 | 56 | 8.2 | 4 | Single | 6 | -- |
| 1-33 | 7 | 65 | 9.5 | 1.5 | Single | 1 | 0.62 |
| 2-19 | 9 | 65 | 9.5 | 1.6 | Split | 7 | 0.75 |
| 0-21 | 3 | 65 | 9.5 | 3.3 | Split | 4 | 0.41 |

* indicates no failure

TABLE S

2400°F Stress Rupture Summary

| Number | Panel | Stress MPa | Stress ksi | Time of Test hours | Failure Type | Number Optical Cracks | Initial Strain Rate |
|---|---|---|---|---|---|---|---|
| 2-24 | 9 | 55 | 8.0 | 270 | * | - | -- |
| 1-40 | 8 | 63 | 9.0 | 117 | * | 7 | -- |
| 0-38 | 5 | 63 | 9.2 | 100 | * | 9 | 0.30 |
| 2-23 | 9 | 63 | 9.3 | 152 | * | 9 | -- |
| 0-29 | 3 | 64 | 9.3 | 1.4 | Single | 10 | 0.78 |
| 1-02 | 6 | 65 | 9.4 | 115 | * | 11 | -- |
| 0-24 | 3 | 65 | 9.4 | 2.2 | Single | 10 | 0.60 |
| 0-26 | 3 | 65 | 9.5 | 1.7 | Single | 9 | 0.78 |
| 2-47 | 11 | 65 | 9.5 | 1.5 | Single | 1 | 0.61 |
| 1-43 | 8 | 65 | 9.5 | 0.9 | Single | 9 | 0.90 |

* indicates no failure

## Appendix C

## Strain Measurement

A four point bend test configuration is employed in the stress rupture test and the strain on a specimen is measured with an extensometry system. A specimen in this test deforms with a curvature and has compressive and tensile strains distributed through the thickness. The radius of curvature is geometrically proportional to the strains in the specimen. The extensometry of the stress rupture test measures the relative displacement of a loaded specimen. The displacement is a factor in a calculation for the radius of curvature and hence the strain. Figure 1C displays the deformation of a specimen into a arc in the flexure test. The specimen has compressive strains at the surface in the concave arc between the load points while the opposite surface is convex and has tensile strains. Between the two exterior surfaces of the specimen, a surface exists without strain and is called the neutral surface. The neutral surface is illustrated by a dashed line in Figure 1C.

The longitudinal strains, $\varepsilon$, on a bend specimen are directly proportional to the radius of curvature, R, at the neutral surface and the distance, y, from the neutral surface by:

$$\varepsilon = \frac{y}{R} \qquad \text{Eq. 1C}$$

Equation 1C is derived solely from the geometry of the test and is independent of the properties of the specimen*. The maximum

---

Timoshenko. S. P., and Gere J. M., Mechanics of Materials, D. Van Nostrand Co., Cincinnati, 1972 pp 113-115.

strain on the specimen occurs at the exterior surfaces because this is the greatest distance from the neutral surface. For all homogeneous material, this distance is one half of the thickness of the specimen.

The maximum strain equation is:

$$\epsilon_{max} = \frac{t}{2R} \qquad \text{Eq. 2C}$$

where t is the thickness of the specimen.

The extensometry of the stress rupture test system is designed to determine the radius of curvature of the loaded specimen. The extensometry probes contact the specimen on the convex side and senses the relative displacement, $d_m$ as in Figure 1C. The radius of curvature on the convex surface is first calculated by an equation derived from the Pythagorian relationship for a right triangle:

$$R_m^2 = L^2 + (R_m - d_m)^2 \qquad \text{Eq. 3C}$$

where $R_m$ and L are the radius of curvature at the convex surface and the distance between the probes respectively and as illustrated in Figure 1C. The value for L is one half inch. Solving Equation 3C for the radius with this value for L yields:

$$R_m = \frac{1/4 + d_m^2}{2d_m} \qquad \text{Eq. 4C}$$

The radius of curvature at the neutral surface can be calculated by subtracting the distance of the neutral to the convex surface from the radius of curvature at the convex surface. The first

approximation of this distance is one half of the thickness of the specimen and this yields:

$$R = R_m - \frac{t}{2} \qquad \text{Eq. 5C}$$

Combining equations 5C, 4C, and 2C yield the strain equation:

$$\varepsilon = \frac{t/2}{\frac{1/4 + d_m^2}{2d_m} - t/2}$$

$$\varepsilon = \frac{t}{\frac{1}{4dm} + dm - t} \qquad \text{Eq. 6C}$$

Equation 6C is employed in the data acquisition system to calculate the strain.

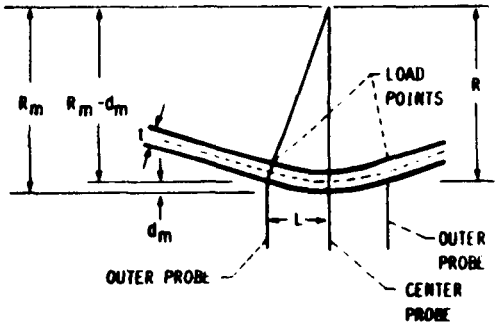


Figure 1C. Bending and Extensometry Geometry.

NASA
National Aeronautics and Space Administration

# Report Documentation Page

| 1. Report No. | 2. Government Accession No. | 3. Recipient's Catalog No. |
|---|---|---|
| NASA CR-180863 | | |

**4. Title and Subtitle**
Stress Rupture Behavior of Silicon Carbide Coated, Low Modulus Carbon/Carbon Composites

**5. Report Date**
January 1988

**6. Performing Organization Code**

**7. Author(s)**
Gary A. Rozak and John F. Wallace

**8. Performing Organization Report No.**
None (E-3708)

**10. Work Unit No.**
505-63-01

**9. Performing Organization Name and Address**
Case Western Reserve University
Dept. of Material Science and Engineering
Cleveland, Ohio 44106

**11. Contract or Grant No.**
NAG3-464

**13. Type of Report and Period Covered**
Contractor Report

**12. Sponsoring Agency Name and Address**
National Aeronautics and Space Administration
Lewis Research Center
Cleveland, Ohio 44135-3191

**14. Sponsoring Agency Code**

**15. Supplementary Notes**
Project Manager, Carl Lowell, Materials Division, NASA Lewis Research Center. This report was a thesis by Gary A. Rozak submitted in partial fulfillment of the requirements for the degree of Master of Science to Case Western Reserve University, January 12, 1988.

**16. Abstract**
The ability of a silicon carbide coated, low modulus, carbon/carbon (c/c) composite to maintain oxidation protection when mechanically loaded has been studied. Low modulus c/c specimens were obtained and the coating was applied in three batches. The differences among the three coating batches and between the bag and mold sides of the composite were determined for density, chemical composition, phase analysis, x-ray radiography, and coating thicknesses. Mechanical tests were conducted in four point bending at room and elevated temperatures of 1000, 1500, 2000, and 2400 °F (538, 816, 1093, and 1316 °C). The flexure strength, proportional limit, and elastic moduli were measured. Stress rupture tests were conducted at the same temperatures and flexural geometries, but were statically loaded until failure or for a maximum of 100 hr. The results of the stress rupture test indicated the existence of a stress rupture limit. The limit increased with increasing temperature from 3.0 ksi (20 Mpa) at 1000 °F to 9.2 ksi (63 MPa) at 2400 °F. Some specimens above the stress rupture limit did not fail while others with equal or lower calculated stresses did fail. This scatter is attributed to material variation. The flexural strength of the coated composite is 12.8 ksi (88 MPa), which is 6 percent less than the uncoated strength of 13.6 ksi (94 MPa). The strength of the coated composite then increased to 13.3 ksi at 2000 °F, and 14.6 ksi (101 MPa) at 2400 °F. The proportional limit observed for the elevated temperature tests increased from 4.0 ksi at 1000 °F to 7.3 ksi (50 MPa) at 2400 °F. The elastic modulus increased over the room temperature value of 3.0 Msi (21 GPa) to 6.0 Msi (41 GPa) at 1000 °F, to 7.0 Msi (48 GPa) at 1500 °F, and then decreased to a value of 6.4 Msi (44 GPa) at 2400 °F. The radiographic examination of the coated composite revealed two different types of texture. Further mechanical examination showed that the differences in the properties between the two types of texture are small. The chemical and physical examination of the composites did not yield differences among the coating batches and between the bag and mold side of the composites. The density of the coating and substrate is 2.6 and 1.4 g/cc, respectively. The coating thickness is 0.014 in. (0.036 cm) on the sides and 0.028 in. (0.071 cm) on the edges. X-ray diffraction analysis of the coating indicated that beta silicon carbide was the major phase. Chemical analysis of the coating indicated that silicon was the major component and that minor amounts of boron, aluminum, and sodium were present.

| 17. Key Words (Suggested by Author(s)) | 18. Distribution Statement |
|---|---|
| Carbon/carbon composites; Stress rupture; Flexure; Elevated temperatures; Coating; Silicon carbide Testing | Unclassified - Unlimited<br>Subject Category 24 |

| 19. Security Classif. (of this report) | 20. Security Classif. (of this page) | 21. No of pages | 22. Price* |
|---|---|---|---|
| Unclassified | Unclassified | 100 | A06 |

NASA FORM 1626 OCT 86

*For sale by the National Technical Information Service, Springfield, Virginia 22161

C-2